TÉCNICO LISBOA

Nonlinear Control of Hybrid Drones via Optimised Control Allocation

Gil Silvestre Serrano

Thesis to obtain the Master of Science Degree in

Electrical and Computer Engineering

Supervisors: Prof. Bruno João Nogueira Guerreiro
Prof. Rita Maria Mendes de Almeida Correia da Cunha

Examination Committee

Chairperson: Prof. João Fernando Cardoso Silva Sequeira
Supervisor: Prof. Bruno João Nogueira Guerreiro
Member of the Committee: Prof. Alexandra Bento Moutinho

January 2021

Declaração

Declaro que o presente documento é um trabalho original da minha autoria e que cumpre todos os requisitos do Código de Conduta e Boas Práticas da Universidade de Lisboa.

Declaration

I declare that this document is an original work of my own authorship and that it fulfils all the requirements of the Code of Conduct and Good Practices of the Universidade de Lisboa.

Acknowledgments

I would like to thank my supervisors, Prof. Bruno Guerreiro and Prof. Rita Cunha, for their untiring support, guidance and insight which have made this dissertation possible, particularly during the unusual circumstances under which it was crafted. A word of gratitude is also in order to José Tojeira for his valuable contribution in the UAV instrumentation.

I wish to also thank my friends and colleagues, in particular Afonso Luís, João Pinto, José Gomes, Renato Dias, and Ricardo Lameirinhas, for their friendship throughout the course and for making this journey far more enjoyable.

Last but not least, I would like to express my profound gratitude to my family, especially to my parents, Alexandre and Fátima, for their unconditional support, encouragement and advice, and to my girlfriend Marta for her love, understanding and motivation.

To each and every one of you – Thank you.

This work was partially funded by the FCT project REPLACE (LISBOA-01-0145-FEDER-032107) which includes Lisboa 2020 and PIDDAC funds, and also projects LARSYS (UIDB/EEA/50009/2020) and CTS (UIDB/EEA/00066/2020).

Abstract

This dissertation addresses the development of a unified control strategy, based on nonlinear control techniques, for hybrid UAVs, more precisely tri-tiltrotor UAVs, so that a simple trajectory is followed. First, the model of a tri-tiltrotor UAV is derived, detailing the forces and moments that act on the system. Then, a unified control approach that considers the system dynamics as a whole is developed. To this effect, backstepping control and nonlinear optimisation are used for position and attitude control to calculate force and moment references. To allocate these references, a control allocation strategy based on nonlinear optimisation is proposed. Next, two trajectories characterised by an upward motion segment and a forward motion segment, each with a different forward velocity value, are defined. In the first trajectory, the UAV is expected to fully transition from rotary-wing to fixed-wing configuration, while in the second trajectory, the objective is to have the UAV fly in an intermediate configuration. To validate the control approach, simulations for the defined trajectories are performed and the results are analysed. Finally, the instrumentation of a tiltrotor UAV is described and verified with a test flight.

Keywords

Hybrid UAV, Tiltrotor UAV, Backstepping control, Control allocation, Trajectory tracking

Resumo

Esta dissertação aborda o desenvolvimento de uma estratégia de controlo unificado, baseada em técnicas de controlo não-linear, para UAVs híbridos, mais precisamente UAVs *tri-tiltrotor*, para que uma trajectória simples seja seguida. Primeiro, o modelo de um UAV tri-tiltrotor é deduzido, detalhando as forças e momentos que actuam sobre o sistema. De seguida, uma estratégia de controlo unificado que considera o sistema como um todo é desenvolvida. Para este efeito, controlo por *backstepping* e técnicas de optimização não-linear são usados para controlo de posição e atitude de modo a calcular referências de força e momento. Para alocar estas referências, uma estratégia de alocação de controlo baseada em optimização não-linear é proposta. São depois definidas duas trajectórias caracterizadas por um segmento vertical e um segmento horizontal, cada uma com velocidade horizontal diferente. Na primeira trajectória, o UAV deverá transitar de uma configuração de asa-rotativa para asa-fixa, enquanto que na segunda trajectória, o objectivo é que o UAV voe numa configuração intermédia. Para validar esta abordagem de controlo, são realizadas simulações para as trajectórias definidas e os resultados são analisados. Por fim, a instrumentação de um UAV *tiltrotor* é descrita e verificada com um vôo de teste.

Palavras Chave

UAV Híbrido, UAV tiltrotor, Controlo por backstepping, Alocação de controlo, Seguimento de trajectória

Contents

List of Figures

Acronyms

3D	three-dimensional
BEC	Battery Elimination Circuit
CoM	centre of mass
ESC	Electronic Speed Controller
NED	North-East-Down
PID	Proportional-Integral-Derivative
PWM	Pulse-Width Modulation
RC	Radio Control
UAV	Unmanned Aerial Vehicle
VTOL	Vertical Take Off and Landing

1

Introduction

Contents

The usage of Unmanned Aerial Vehicles (UAVs) has grown considerably over the past years as more applications, whether military, civilian or in academia, are found for these vehicles. Depending on the nature of the application, the type of UAV that has the best performance for a certain task may vary. Fixed-wing and rotary-wing UAVs are ubiquitous. Despite their predominance, both types of UAV are not without flaw. Each presents a distinct set of advantages and disadvantages. A different type of UAV attempts to mitigate the shortcomings and combine the strengths of both fixed-wing and rotary-wing aircraft - hybrid UAVs. These UAVs are typically fixed-wing vehicles with Vertical Take Off and Landing (VTOL) capabilities, which enables them to be more effective in a wider range of application scenarios. However, hybrid UAVs are complex vehicles and therefore pose additional challenges in modelling and control.

1.1 Motivation

The motivation for this dissertation stems from the opportunity to take advantage of the characteristics of hybrid UAVs in applications in which fixed and rotary-wing UAVs do not perform as adequately.

This dissertation was developed within the scope of the REPLACE project [1], which intends to develop a package delivery system in urban environments using UAVs. This project addresses the problem of vehicle autonomy and flight distance by exchanging parcels between UAVs, thus extending the possible delivery range. This presents a plethora of challenges in, for example, cooperative control of a heterogeneous UAV system, flight and manoeuvre control for package exchange, path planning and following, trajectory tracking, as well as logistics optimisation. Hybrid UAVs offer some features, such as improved range, manoeuvrability and the ability to vertically take off in a confined environment, which would be beneficial for such a delivery system.

1.2 Objectives

This dissertation addresses the design of nonlinear control techniques for trajectory tracking with hybrid UAVs, more precisely, tiltrotor UAVs.

The usual control approach for hybrid vehicles is to employ hybrid control techniques, defining several modes of working that are less complex than the entire system, developing controllers for each mode, and switching between them as required to control the vehicle. In the case of hybrid UAVs, a common approach is to consider a rotary-wing or multicopter mode and a fixed-wing mode, as is the case of control strategy the PX4 autopilot for this type of vehicles, as depicted in Figure 1.1. One of the objectives of this dissertation is to take the initial steps towards a unified control approach to tiltrotor UAVs, considering the system as a whole, instead of having different modes of operation, as will

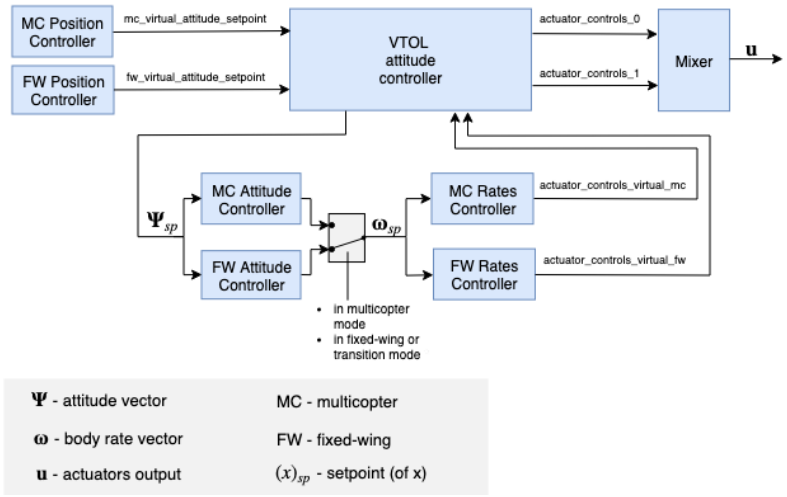

Figure 1.1: PX4 autopilot's hybrid control approach diagram (from [2])

be seen. By not dividing the system into different modes, another goal is to have the UAV fly in an intermediate configuration, neither fully in rotary-wing nor in fixed-wing mode.

1.3 Proposed Approach and Dissertation Outline

To achieve the aforementioned objectives, the model of a tiltrotor UAV will be derived. Next, the unified nonlinear control strategy, based on backstepping control, will be designed. Then, simple trajectories that take the aircraft up to a certain altitude to then begin flying forward are described and the control approach is tested in simulation to check if the vehicle behaves as intended and flies in the expected configurations. The remainder of this dissertation is organised as follows:

– Chapter 2 provides a brief overview of hybrid aircraft, with an emphasis on tiltrotor UAVs, and a review of research on hybrid UAVs.

– Chapter 3 gives the theoretical background on orientation representation and backstepping control.

– Chapter 4 describes the nonlinear model of a tilrotor UAV, defining the necessary coordinate frames, characterising the forces and moments generated by the rotors and by aerodynamics, and deriving the error dynamics.

– Chapter 5 delineates the unified control approach, using backstepping to control the position and attitude of the UAV, as well as the control allocation scheme, based on nonlinear optimisation.

– Chapter 6 addresses the composition of the reference trajectories and presents the simulation results and the evaluation of the performance.

– Chapter 7 describes the instrumentation of a tiltrotor UAV.

– Chapter 8 summarises the work developed in this dissertation and assesses what is still to be done as future work.

2

Related Work

Contents

In this chapter, we present an overview of hybrid aircraft, followed by a more detailed approach to tiltrotor UAV. Then, we cover the research that has been conducted on design, modelling and control of hybrid UAV.

2.1 Hybrid Aircraft

There are two major types of aircraft, fixed-wing and rotary-wing, each with their set of advantages and disadvantages. Fixed-wing aircraft are able to achieve greater speed, have a longer flight range, and can carry a heavy weight. However, due to their configuration and how lift is generated, they are not able to fly at low speed nor hover, which limits their applicability to situations in restricted surroundings. In addition, these aircraft also require runways or dedicated apparatus for taking off and landing. Rotary-wing aircraft, on the other hand, present greater flexibility in confined areas, due to the ability to hover and having less restraints for taking off and landing, at the cost of lower flight speed and range.

Hybrid aircraft combine features of fixed-wing and rotary-wing aircraft in order to take advantage of the best performance aspects of both types of vehicles and lessen the drawbacks. The ability to fly at high speeds, with a long flight range and greater payload capacity, coupled with the possibility to vertically take off and land without a runway, give hybrid aircraft more manoeuvrability and a wider range of application scenarios than fixed-wing or rotary-wing aircraft. The operation of these aircraft is usually divided into three modes: hover, transition, and cruise flight.

Aircraft with such characteristics were of interest to military organisations. The first attempts at developing a hybrid aircraft were conducted by the United States Navy in the 1950's, which resulted in the Lockheed XFV, Figure 2.1(a), and Convair XFY, Figure 2.1(b). These were tailsitter aircraft, with counter-rotating propellers, which were difficult to fly, lacked speed and lifting power, among other problems, and the projects were terminated [3, 4]. Further developments kept being driven by military organisations, with more types of hybrid aircraft being designed and tested during the following decades. One such aircraft was the Bell Boeing V22 Osprey, Figure 2.1(c), a highly successful bi-tiltrotor aircraft developed in the 1980's, which is still in use [5]. More recently, the attention of military organisations has shifted to hybrid UAV. For example, the Portuguese Navy and UAVision have partnered to develop the *Ogassa OGS42V*, Figure 2.1(d), a dual-system UAV for maritime operations, as the ability to take off and land vertically is advantageous for use on a ship [6].

In the past decade, hybrid aircraft, more specifically hybrid UAV, have increasingly been the target of academic research, as well as civilian enterprises. Research groups have been working on problems such as design and manufacturing, modelling, control, guidance and navigation, and robustness [7]. As an example of such research, a quad-tailsitter UAV, *VertiKUL*, Figure 2.2(a), was developed at KU Leuven, for the purpose of package delivery [8]. A more recent project, *Maribot Kungsfiskare*, is being

(a) Lockheed XFV (from [3])

(b) Convair XFY (from [4])

(c) Bell Boeing V22 (from [5])

(d) Ogassa VTOL (from [6])

Figure 2.1: Military Hybrid Aircraft

developed at KTH with a tri-tiltrotor UAV, Figure 2.2(b), to be used in maritime environments [9].

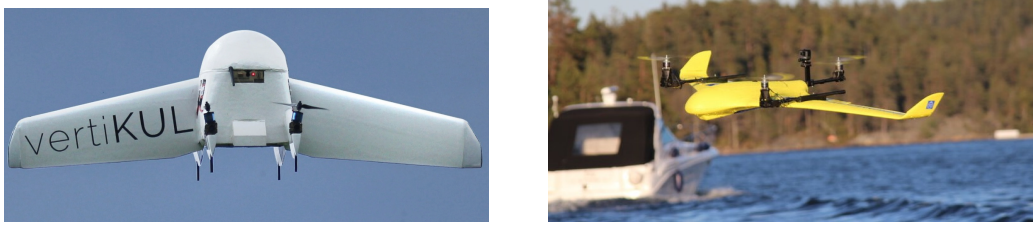

(a) VertiKUL (from [8])

(b) Maribot Kungsfiskare (from [9])

Figure 2.2: Hybrid UAVs developed by academic research groups

Regarding civilian applications of hybrid UAV, DHL and Wingcopter have recently partnered to develop *Parcelcopter 4.0* [10], Figure 2.3(a), a quad-tiltrotor hybrid UAV, to deliver medication and medical supplies in the Lake Victoria region, to lessen the effects of poor road networks. The ability to vertically take off and land is key in regions were infrastructure is limited, and the high speed achieved in cruise flight allows to deliver vital supplies, which would otherwise take more than 4 hours, in approximately 40 minutes. The previous stage of this project, *Parcelcopter 3.0*, employed a different kind of hybrid aircraft, a tiltwing UAV, Figure 2.3(b).

There are several types of hybrid aircraft, some have already been mentioned, such as tiltrotor, tiltwing, tailsitter, dual-system, and more. In this dissertation, the focus will be on tiltrotor UAVs.

(a) Parcelcopter 4.0 (from [10])

(b) Parcelcopter 3.0 (from [10])

Figure 2.3: DHL Parcelcopter Hybrid UAVs

2.1.1 Tiltrotor Unmanned Aerial Vehicles

Tiltrotor UAVs have rotors mounted on tilting shafts, which are pointed upwards in hover mode and tilt forward during the transition to cruise flight in order to provide forward speed. There are three principal

configurations of tiltrotor UAVs: bi-tiltrotor, tri-tiltrotor, and quad-tiltrotor [7, 11].

A bi-tiltrotor UAV employs two tilting rotors to provide lift in hover and thrust in cruise. In hover mode, roll is controlled by differential thrust, pitch by the forward longitudinal cyclic pitch produced by the forward tilting of the rotors and yaw by thrust vectoring. In cruise mode, these aircraft function similarly to fixed-wing aircraft, with the thrust being provided by the rotors tilted forward, and roll, pitch and yaw being controlled by control surfaces [7].

Tri-tiltrotor UAVs usually incorporate two front tilting rotors and one fixed rotor in the rear area, directed upwards. In hover mode, all three rotors are directed upwards. During the transition, the two front rotors tilt forward to generate thrust and accelerate forward. Just as in the previous configuration, a tri-tiltrotor UAV behaves akin to a fixed-wing aircraft in cruise flight mode, with the tail rotor stopped. In comparison to bi-tiltrotor UAVs, the addition of one more rotor reduces the required lift generated by each rotor in hover mode [7, 12].

The quad-tiltrotor configuration, as the name implies, possesses four tilting rotors. In hover mode, these vehicles work similarly to quadcopters, with better yaw control due to the possibility of tilting the rotors. During the transition to cruise flight mode, the front rotors tilt forward and the back rotors stop (and in some cases are retracted), after which the UAV operates like a fixed-wing aircraft [7, 13].

The type of UAV that is going to be modelled in this dissertation is a tri-tiltrotor UAV. It is going to be based on the *E-Flite Convergence VTOL*, Figure 2.4, which has two front tilting rotors, a fixed tail rotor, and two elevons. Elevons are control surfaces that produce the same effect as an elevator, if driven together, and the same effect of ailerons, if driven differentially.

Figure 2.4: E-Flite Convergence VTOL

2.2 Literature Review

As aforementioned, the past decade has seen an increase in research work on hybrid UAVs. Much work is focused on developing control algorithms that target one of the operation modes of these vehicles,

while others opt for a more comprehensive approach to the problem. Control methods for hybrid UAVs usually employ hybrid control techniques, which consist of designing controllers for each operation mode and switching between them, while guaranteeing that the system remains stable during the transition.

A hybrid approach to the control of a quad-tiltrotor is explored in [13], in which the problem is broken down into the sequence of hover, transition, cruise level flight, and transition back to hover. The aircraft's dynamics for the hover mode and cruise mode are deduced and nonlinear control strategies are derived for each mode. The control performance was evaluated in simulation and then experimentally on a prototype for the hover mode. The work is continued in [14], which focuses on the transition from hover to cruise flight of the same quad-tiltrotor UAV. The manoeuvre is defined so that the altitude remains constant throughout the transition. Therefore, the total thrust must compensate for the UAV's weight to maintain the altitude and increase the aircraft speed. To control the transition, a control strategy based on Lyapunov design is derived, which ensures global stability for the altitude and local stability for the forward velocity. Simulation results demonstrated the desired behaviour, with the transition manoeuvre taking approximately one second.

Another hybrid approach, that uses gain-scheduling, has been developed for the longitudinal control of a bi-tiltrotor UAV [15]. As such, the longitudinal dynamics model is derived and the aerodynamic coefficients are calculated via wind tunnel tests. The simulated trajectory consists of hovering at a certain altitude and transitioning to cruise level flight. The rotor's tilt angle is computed by an altitude dependent function. The aircraft performs the transition, but the gain-scheduling controller is not able to keep it at a constant altitude, which increases as the UAV flies forward.

Regarding tri-tiltrotor UAVs, in [12], the dynamical model of the aircraft is divided into two situations: in hover mode, in which aerodynamic effects are neglected, and in cruise flight mode, with a simplified model of the aerodynamic effects. The control strategy takes into account the longitudinal dynamics for altitude and attitude control, i.e. only pitch motion is stabilised by the controller, with roll and yaw being controlled manually. Control is achieved with an adaptive Proportional-Integral-Derivative (PID) controller, whose parameters are tuned by a neural network to obtain more accurate control over the entire trajectory and minimise the effects of disturbances. The defined trajectory has a trapezoidal velocity profile, meaning that the aircraft accelerates at a constant value until a certain velocity is reached, maintaining that velocity until it start decelerating also at a constant value. This type of trajectory was also adopted in [16], with the objective of producing a smooth motion, as it is simple and constrains the maximum velocity and acceleration.

The modelling and control of a tri-tiltrotor UAV is also the subject of [17], though only for hover mode. As such, the aerodynamic effects, important in this kind of aircraft, are not modelled. An attitude PID controller and a control allocation scheme based on the desired roll and pitch moments and (vertical) thrust are designed and implemented. The system is then tested in simulation and experimentally with

adequate results in altitude stability, despite the more oscillatory behaviour in terms of attitude control.

A more complete nonlinear model of a tri-tiltrotor UAV is derived in [18], with emphasis on the transition dynamics. Aerodynamic effects with respect to cruise speed, rotor's tilt angle and angle of attack are studied in computational fluid dynamics simulation. The same method is employed to compute the aerodynamic coefficients of the UAV. Then, with the information gathered in simulation, a hybrid approach that switches between hover, transition and cruise flight controllers is implemented and tested in simulation. With a trajectory beginning in hover, transitioning to cruise flight and then back to hover, the aircraft is not able to maintain the altitude, decreasing further with every controller switch. The attitude, in particular the pitch angle, shows oscillatory behaviour at each controller switch.

Unified approaches to control of hybrid UAV have also been developed, in lieu of hybrid approaches, although not as common as the latter. In [19], the flight envelope of a tiltwing UAV is studied and modelled via wind tunnel tests, which makes it possible to define a continuous flight configuration space that contains the different flight modes (hover, transition and cruise flight), thus not needing to define discrete flight configurations. As such, the three flight modes comprise a trajectory defined within the flight envelope. With this strategy, a map-based feedforward controller that used virtual control inputs independent of the flight state for motion control is developed. The tilt angle of the wing is considered as a configuration parameter, obtained in conjunction with the aircraft's pitch angle, dependent on the flight state. The approach in [20], for a quad-tailsitter UAV, handles the flight modes in a continuous fashion as well. Unlike the previous example of a tiltwing, in the case of a tailsitter, the aircraft's attitude changes significantly across the flight envelope, as there is no tilting mechanism to change the direction of the thrust generated by the rotors. To deal with this issue, the controller solves a nonlinear optimisation problem, which computes the required attitude and thrust to achieve the desired acceleration set by the position controller. The attitude and thrust are then fed to the attitude controller designed to be globally asymptotically stable. As an accurate model of the UAV's flight envelope is of significant importance, wind tunnel tests were also conducted.

In July 2020, Auterion announced at the PX4 Developer Summit that they are developing a novel approach to control allocation based on dynamic computation of input effectiveness matrices [21]. The motivation behind this technique is linked to fault tolerant control. Moreover, it was shown to allow a single form of control allocation for hybrid UAV, instead of different control allocation schemes for each flight mode. This method's performance was demonstrated with an *E-Flite Convergence VTOL*, which was able to fly in an intermediate mode, not fully in hover nor cruise flight. There are still many limitations with this approach for hybrid UAV, since the effectiveness matrix calculation is done by linearising the input influence on the dynamics around a constant trim point. As such, the aircraft cannot fly in cruise flight and there are constraints on the rotors' tilt angle due to the linearisation not being valid in every flight mode. Nonetheless, it is a considerable step towards a unified control structure for tiltrotor UAV.

3

Theoretical Background

Contents

In this chapter, we present the theoretical concepts applied throughout this dissertation. First, an overview of rotation representation with Euler angles and with quaternions is made. Then, the basis of backstepping control is laid out. Finally, the concept of trim trajectories is introduced.

3.1 Orientation Representation

It will be of interest to represent the three-dimensional (3D) orientation of a moving frame $\{\mathcal{B}\}$ of an aircraft's body with respect to a fixed inertial frame $\{\mathcal{I}\}$. These frames will be explained in detail in Chapter 4. There is a number of possible ways to represent orientation and rotation, but here we focus on two: Euler angles and quaternions. The information presented in this section is based on [22, 23].

3.1.1 Euler Angles

Euler angles are a commonly used representation of orientation. It consists of a vector of three angles $\begin{bmatrix}\phi & \theta & \psi\end{bmatrix}^\mathsf{T}$ that each represent a rotation about an axis of a moving frame in relation to a stationary frame, such that the location of the axis of each rotation depends on the succession of previous rotations. Therefore, the order of the rotations must be defined as well to fully describe the orientation. A frequent choice of rotation order is $Z-Y-X$, from $\{\mathcal{I}\}$ to $\{\mathcal{B}\}$, in which there is first a rotation of ψ (yaw) about the $\hat{z}$-axis of the body frame, followed by a rotation of θ (pitch) about the $\hat{y}$-axis, and concludes with a rotation of ϕ (roll) about the $\hat{x}$-axis. Each of these elementary rotations may be written in the form of rotation matrices as

$$\mathbf{R}_{\hat{x}} = \begin{bmatrix} 1 & 0 & 0 \\ 0 & \cos(\phi) & \sin(\phi) \\ 0 & -\sin(\phi) & \cos(\phi) \end{bmatrix}, \quad \mathbf{R}_{\hat{y}} = \begin{bmatrix} \cos(\theta) & 0 & -\sin(\theta) \\ 0 & 1 & 0 \\ \sin(\theta) & 0 & \cos(\theta) \end{bmatrix}, \quad \mathbf{R}_{\hat{z}} = \begin{bmatrix} \cos(\psi) & \sin(\psi) & 0 \\ -\sin(\psi) & \cos(\psi) & 0 \\ 0 & 0 & 1 \end{bmatrix} \tag{3.1}$$

The group of 3D rotations is the special orthogonal group $\mathrm{SO}(3)$. The matrices in (3.1), as well as any 3-by-3 rotation matrix, represent transformations that are part of this group. These matrices are thus known as orthogonal matrices. The properties $\mathbf{R}^\mathsf{T} = \mathbf{R}^{-1}$ and $\det(\mathbf{R}) = 1$ are true for any such matrix $\mathbf{R} \in \mathrm{SO}(3)$.

Multiplying the matrices in (3.1) in the right order gives the rotation matrix ${}^{\mathcal{B}}_{\mathcal{I}}\mathbf{R}$, which represents the orientation of $\{\mathcal{I}\}$ relative to $\{\mathcal{B}\}$. If the succession of elementary rotations is done in the $Z-Y-X$ order, then ${}^{\mathcal{B}}_{\mathcal{I}}\mathbf{R}$ is given by

$$\begin{aligned} {}^{\mathcal{B}}_{\mathcal{I}}\mathbf{R} &= \mathbf{R}_{\hat{x}}\,\mathbf{R}_{\hat{y}}\,\mathbf{R}_{\hat{z}} \\ &= \begin{bmatrix} \cos(\psi)\cos(\theta) & \sin(\psi)\cos(\theta) & -\sin(\theta) \\ \cos(\psi)\sin(\theta)\sin(\phi) - \sin(\psi)\cos(\phi) & \sin(\psi)\sin(\theta)\sin(\phi) + \cos(\psi)\cos(\phi) & \cos(\theta)\sin(\phi) \\ \cos(\psi)\sin(\theta)\cos(\phi) + \sin(\psi)\sin(\phi) & \sin(\psi)\sin(\theta)\cos(\phi) - \cos(\psi)\sin(\phi) & \cos(\theta)\cos(\phi) \end{bmatrix}, \end{aligned} \tag{3.2}$$

A problem with this representation is connected to the calculation of the Euler angles' time derivatives $\begin{bmatrix}\dot{\phi} & \dot{\theta} & \dot{\psi}\end{bmatrix}^{\mathsf{T}}$ from the aircraft's angular velocity $\boldsymbol{\omega}$. This calculation is done by

$$\begin{bmatrix}\dot{\phi}\\ \dot{\theta}\\ \dot{\psi}\end{bmatrix} = \begin{bmatrix}1 & \sin(\phi)\tan(\theta) & \sin(\phi)\tan(\theta)\\ 0 & \cos(\phi) & -\sin(\phi)\\ 0 & \sin(\phi)/\cos(\theta) & \cos(\phi)/\cos(\theta)\end{bmatrix}\boldsymbol{\omega}\,. \tag{3.3}$$

By analysing the matrix in (3.3), one concludes that there are singularities at $\theta = \pm\frac{\pi}{2}$, meaning that the problem is undefined for these values of θ.

3.1.2 Quaternions

Quaternions are a four-dimensional number system, with one scalar dimension and three imaginary dimensions, whose properties motivate its application to 3D rotations. A quaternion $\boldsymbol{q}$ has four scalar components $(q_0,\, q_1,\, q_2,\, q_3)$ and is given by

$$\boldsymbol{q} = q_0 + q_1\boldsymbol{i} + q_2\boldsymbol{j} + q_3\boldsymbol{k} = (q_0,\, \mathbf{q})\,, \tag{3.4}$$

where $\boldsymbol{i}$, $\boldsymbol{j}$, $\boldsymbol{k}$ are the basis units for each imaginary dimension which follow

$$\boldsymbol{i}^2 = \boldsymbol{j}^2 = \boldsymbol{k}^2 = \boldsymbol{ijk} = -1\,. \tag{3.5}$$

The representation $(q_0,\, \mathbf{q})$, which will be more often used in this dissertation, divides the quaternion into a scalar part $q_0 \in \mathbb{R}$ and a vector part $\mathbf{q} = \begin{bmatrix}q_1 & q_2 & q_3\end{bmatrix}^{\mathsf{T}} \in \mathbb{R}^3$.

The product of two quaternions $\boldsymbol{p} = (p_0,\, \mathbf{p})$ and $\boldsymbol{q} = (q_0,\, \mathbf{q})$, represented by $\boldsymbol{p} \circ \boldsymbol{q}$, is defined as

$$\boldsymbol{p} \circ \boldsymbol{q} = (p_0\, q_0 - \mathbf{p}\cdot\mathbf{q}\,,\, p_0\,\mathbf{q} + q_0\,\mathbf{p} + \mathbf{p}\times\mathbf{q})\,. \tag{3.6}$$

Note that quaternion multiplication is non-commutative, i.e. $\boldsymbol{p} \circ \boldsymbol{q} \neq \boldsymbol{q} \circ \boldsymbol{p}$. The norm of a quaternion is given by

$$\|\boldsymbol{q}\| = \sqrt{q_0^2 + q_1^2 + q_2^2 + q_3^2}\,. \tag{3.7}$$

The quaternion conjugate is given by

$$\bar{\boldsymbol{q}} = (q_0,\, -\mathbf{q})\,. \tag{3.8}$$

From the aforementioned properties, it follows that the product of a quaternion by its conjugate is

$$\boldsymbol{q} \circ \bar{\boldsymbol{q}} = (\|\boldsymbol{q}\|^2,\, \mathbf{0})\,. \tag{3.9}$$

When considering quaternions in the context of 3D rotations, it is usual to restrict the analysis to unit

quaternions, i.e. quaternions such that $\|\boldsymbol{q}\| = 1$. These quaternions are points on the unit 3-sphere $\mathbb{S}^3$. Unit quaternions are isomorphic to the special unitary group $\mathrm{SU}(2)$, while 3D rotations comprise the special orthogonal group $\mathrm{SO}(3)$, meaning there is a 2 to 1 surjective homomorphism between unit quaternions and 3D rotations. This implies that, given a rotation matrix, there is ambiguity regarding the corresponding quaternion, as two quaternions map to that matrix. As will be seen below, if one such quaternion is $\boldsymbol{q}$, the other is $-\boldsymbol{q}$.

According to Euler's Theorem, 3D rotations can be described by rotating by an angle α about an axis represented by a (unit) vector $\hat{\mathbf{n}}$. As aforementioned, a quaternion may be characterised by a scalar and a vector part, which is what is needed to describe 3D rotations. Hence, a rotation of α about $\hat{\mathbf{n}} = \begin{bmatrix} n_x & n_y & n_z \end{bmatrix}^\mathsf{T}$ may be represented by

$$\boldsymbol{q} = \cos\frac{\alpha}{2} + \sin\frac{\alpha}{2}\left(n_x\boldsymbol{i} + n_y\boldsymbol{j} + n_z\boldsymbol{k}\right), \tag{3.10}$$

which means $q_0 = \cos\frac{\alpha}{2}$, $q_1 = n_x \sin\frac{\alpha}{2}$, $q_2 = n_y \sin\frac{\alpha}{2}$, and $q_3 = n_z \sin\frac{\alpha}{2}$. To obtain the rotation of a vector $\mathbf{u}$, using quaternions, we consider $\boldsymbol{u} = (0,\, \mathbf{u})$ and perform

$$\boldsymbol{u}' = \boldsymbol{q} \circ \boldsymbol{u} \circ \bar{\boldsymbol{q}} = (0,\, \mathbf{u}') = (0,\, \mathbf{R}(\boldsymbol{q})\,\mathbf{u}) \tag{3.11}$$

where $\mathbf{u}'$ is the rotated vector, and the rotation matrix $\mathbf{R}(\boldsymbol{q})$ is

$$\mathbf{R}(\boldsymbol{q}) = \begin{bmatrix} q_0^2 + q_1^2 - q_2^2 - q_3^2 & 2q_1q_2 - 2q_0q_3 & 2q_1q_3 + 2q_0q_2 \\ 2q_1q_2 + 2q_0q_3 & q_0^2 - q_1^2 + q_2^2 - q_3^2 & 2q_2q_3 - 2q_0q_1 \\ 2q_1q_3 - 2q_0q_2 & 2q_0q_1 + 2q_2q_3 & q_0^2 - q_1^2 - q_2^2 + q_3^2 \end{bmatrix}. \tag{3.12}$$

Since every element in $\mathbf{R}(\boldsymbol{q})$ only has terms that are quadratic in the elements of $\boldsymbol{q}$, it follows that $\mathbf{R}(\boldsymbol{q}) = \mathbf{R}(-\boldsymbol{q})$, i.e. both $\boldsymbol{q}$ and $-\boldsymbol{q}$ map to the same rotation matrix. If $\boldsymbol{q}$ is the quaternion that represents the orientation of $\{\mathcal{B}\}$ relative to $\{\mathcal{I}\}$, then the rotation matrix $\mathbf{R}(\boldsymbol{q})$ corresponds to ${}^{\mathcal{I}}_{\mathcal{B}}\mathbf{R}$.

The aforementioned Euler angles $\begin{bmatrix} \phi & \theta & \psi \end{bmatrix}^\mathsf{T}$ can be calculated from the quaternion $\boldsymbol{q}$ above by

$$\begin{aligned} \phi &= \mathrm{atan2}\left(2(q_0q_1 + q_2q_3),\, q_0^2 - q_1^2 - q_2^2 + q_3^2\right), \\ \theta &= \mathrm{asin}\left(2(q_0q_2 - q_1q_3)\right), \\ \psi &= \mathrm{atan2}\left(2(q_0q_3 + q_1q_2),\, q_0^2 + q_1^2 - q_2^2 - q_3^2\right). \end{aligned} \tag{3.13}$$

Conversely, the quaternion $\boldsymbol{q}$ can be calculated from the Euler angle by

$$
\begin{aligned}
q_0 &= \cos\frac{\psi}{2}\cos\frac{\theta}{2}\cos\frac{\phi}{2} + \sin\frac{\psi}{2}\sin\frac{\theta}{2}\sin\frac{\phi}{2}\,, \\
q_1 &= \cos\frac{\psi}{2}\cos\frac{\theta}{2}\sin\frac{\phi}{2} - \sin\frac{\psi}{2}\sin\frac{\theta}{2}\cos\frac{\phi}{2}\,, \\
q_2 &= \cos\frac{\psi}{2}\sin\frac{\theta}{2}\cos\frac{\phi}{2} + \sin\frac{\psi}{2}\cos\frac{\theta}{2}\sin\frac{\phi}{2}\,, \\
q_3 &= \sin\frac{\psi}{2}\cos\frac{\theta}{2}\cos\frac{\phi}{2} - \cos\frac{\psi}{2}\sin\frac{\theta}{2}\sin\frac{\phi}{2}\,.
\end{aligned}
\tag{3.14}
$$

3.2 Backstepping Control

Backstepping is a state feedback nonlinear control technique. It is a recursive process that aims at progressively deriving linearising control laws that stabilise inner subsystems and ”back step” until the external control is reached to then make the entire system stable. This method requires a good knowledge of the system model and is sensitive to parameter uncertainty. This section is adapted from [24–26], which cover the subject more comprehensively. Let us consider a nonlinear system of the form

$$
\begin{aligned}
\dot{x} &= f_a(x) + g_a(x)\,\xi \\
\dot{\xi} &= f_b(x,\xi) + g_b(x,\xi)\,u
\end{aligned}
\tag{3.15}
$$

with state variables $x \in \mathbb{R}^n$ and $\xi \in \mathbb{R}$, and control input $u \in \mathbb{R}$. System (3.15) can be interpreted as two cascaded subsystems with ξ being the input to the first and u the input to the second, which is controlled directly. Therefore, we begin by designing a state feedback controller $\xi = \alpha(x)$, with $\alpha(0) = 0$, that stabilises the first subsystem, and considering a Lyapunov function $V_1(x)$ such that

$$
\dot{V}_1 = \frac{\partial V_1}{\partial x}\left(f_a(x) + g_a(x)\,\alpha(x)\right) < 0\,. \tag{3.16}
$$

Then, introducing a new variable $y = \xi - \alpha(x)$, system (3.15) can be rewritten as

$$
\begin{aligned}
\dot{x} &= f_a(x) + g_a(x)\,\alpha(x) + g_a(x)\,y \\
\dot{y} &= f_b(x,\xi) - \frac{\partial \alpha}{\partial x}\left(f_a(x) + g_a(x)\,\alpha(x) + g_a(x)\,y\right) + g_b(x,\xi)\,u\,.
\end{aligned}
\tag{3.17}
$$

From (3.17), it follows that if u is designed such that y is driven to and stabilised at zero, then the full system is, as a consequence, stabilised as well. Defining a candidate Lyapunov function $V_2(x,\xi)$ as being

$$
V_2(x,\xi) = V_1(x) + \frac{1}{2}y^2\,. \tag{3.18}
$$

With this function, we design the control law for input u by first taking the time-derivative and setting it to

be less or equal to zero, which yields

$$\dot{V}_2(x,\xi) = \dot{V}_1 + \frac{\partial V_1}{\partial x}\, g_a(x)\, y + y\, \left(f_b(x,\xi) - \frac{\partial \alpha}{\partial x}\, (f_a(x) + g_a(x)\, \alpha(x) + g_a(x)\, y) + g_b(x,\xi)\, u \right) \leq 0\,. \quad (3.19)$$

Thus, the control input u that achieves this objective is given by

$$u = -\frac{1}{g_b(x,\xi)} \left(\frac{\partial V_1}{\partial x} g_a(x) + f_b(x,\xi) - \frac{\partial \alpha}{\partial x}\, (f_a(x) + g_a(x)\, \alpha(x) + g_a(x)\, y) + k\, (\xi - \alpha(x)) \right)\,. \quad (3.20)$$

This example features two subsystems, but this technique, due to its recursive nature, may be used in higher dimensional systems, without necessarily increasing the complexity.

4

Tiltrotor Modelling

Contents

This chapter presents the modelling concepts used throughout this dissertation. First, the coordinate frames are defined. Then, the aerodynamic and rotor forces and moments are introduced. Afterwards, the rigid-body kinematics and Newton-Euler equations are derived, thus arriving at the model for the hybrid tiltrotor UAV. Finally, the error dynamics are deduced.

4.1 Coordinate Frames

To define the rigid-body kinematics and dynamics, it is first necessary to define an inertial frame of reference $\{\mathcal{I}\}$, which in this case will be earth-fixed, and a body-fixed frame $\{\mathcal{B}\}$.

An inertial reference frame is a coordinate frame in which the net force acting on it, i.e. net acceleration, is zero. A point on the earth's surface will experience centripetal acceleration due to the earth's rotation, which may be ignored, on the account of its small magnitude when compared to the gravitational acceleration. Since a UAV has a velocity much lower when compared to the earth's rotational velocity, it is typical to approximate the earth by a local tangent plane (flat Earth approximation). A coordinate system commonly used in literature for this type of reference frame is the North-East-Down (NED) coordinate system [27, 28]. The origin of this frame is a fixed point on the earth's surface $O_{\mathcal{I}}$, the x-axis, represented by unit vector $\hat{\boldsymbol{\imath}}_{\mathcal{I}}$, points north, the y-axis, $\hat{\boldsymbol{\jmath}}_{\mathcal{I}}$, points east, and the z-axis, $\hat{\boldsymbol{k}}_{\mathcal{I}}$, points towards the earth in the direction of the plane's normal. Thus, the inertial frame is defined as a NED coordinate system $\{\mathcal{I}\} = \{O_{\mathcal{I}};\ \hat{\boldsymbol{\imath}}_{\mathcal{I}},\ \hat{\boldsymbol{\jmath}}_{\mathcal{I}},\ \hat{\boldsymbol{k}}_{\mathcal{I}}\}$.

The body-fixed frame $\{\mathcal{B}\} = \{O_{\mathcal{B}};\ \hat{\boldsymbol{\imath}}_{\mathcal{B}},\ \hat{\boldsymbol{\jmath}}_{\mathcal{B}},\ \hat{\boldsymbol{k}}_{\mathcal{B}}\}$ is necessary to describe the relative motion of the aircraft. This frame is defined by having its origin on the centre of mass (CoM) of the vehicle, denoted by $O_{\mathcal{B}}$, the x-axis, $\hat{\boldsymbol{\imath}}_{\mathcal{B}}$, pointing forward, the y-axis, $\hat{\boldsymbol{\jmath}}_{\mathcal{B}}$, pointing to the right, and the z-axis, $\hat{\boldsymbol{k}}_{\mathcal{B}}$, pointing downward, also a common convention in literature [28].

As mentioned in Chapter 2, the hybrid UAV that is going to be analysed and used throughout this dissertation is classified as a tri-tiltrotor. It includes two tilting rotors, one on each wing, with one degree of freedom, i.e. rotors that tilt longitudinally in a pitching motion, and one fixed rotor on the tail of the UAV that generates thrust perpendicularly to the $\hat{\boldsymbol{\imath}}_{\mathcal{B}} - \hat{\boldsymbol{\jmath}}_{\mathcal{B}}$ plane. As such, following the approach in [29], two more coordinate frames $\{\mathcal{T}_1\}$ and $\{\mathcal{T}_2\}$ are introduced, one for each tilting rotor.

Assigning $\{\mathcal{T}_1\} = \{O_{\mathcal{T}_1};\ \hat{\boldsymbol{\imath}}_{\mathcal{T}_1},\ \hat{\boldsymbol{\jmath}}_{\mathcal{T}_1},\ \hat{\boldsymbol{k}}_{\mathcal{T}_1}\}$ to the right wing rotor, with x-axis $\hat{\boldsymbol{\imath}}_{\mathcal{T}_1}$ aligned along the rotation axis, pointing forward, y-axis $\hat{\boldsymbol{\jmath}}_{\mathcal{T}_1}$ aligned with the tilting axis, pointing right, and z-axis $\hat{\boldsymbol{k}}_{\mathcal{T}_1}$ pointing downward (when the rotor is tilted forward). The origin $O_{\mathcal{T}_1}$ is thus defined as the point where the rotor spin and tilting axes intersect and the generated force is applied. The coordinate frame $\{\mathcal{T}_2\} = \{O_{\mathcal{T}_2};\ \hat{\boldsymbol{\imath}}_{\mathcal{T}_2},\ \hat{\boldsymbol{\jmath}}_{\mathcal{T}_2},\ \hat{\boldsymbol{k}}_{\mathcal{T}_2}\}$ for the left wing rotor is defined similarly. The positions of the origins of $\{\mathcal{T}_1\}$ and $\{\mathcal{T}_2\}$, with respect to the body frame $\{\mathcal{B}\}$, are denoted by $\mathbf{r}_1 = \begin{bmatrix} r_{1,x} & r_{1,y} & r_{1,z} \end{bmatrix}^{\mathsf{T}}$ and $\mathbf{r}_2 = \begin{bmatrix} r_{2,x} & r_{2,y} & r_{2,z} \end{bmatrix}^{\mathsf{T}}$, respectively. The two front rotors over the wings of the aircraft can rotate

independently. Let γ_1 and γ_2 denote the angle rotated by the right and left rotors, respectively. The orientations of $\{\mathcal{T}_1\}$ and $\{\mathcal{T}_2\}$ relative to $\{\mathcal{B}\}$ are given by the rotation matrices ${}^{\mathcal{B}}_{\mathcal{T}_1}\mathbf{R}(\gamma_1)$ and ${}^{\mathcal{B}}_{\mathcal{T}_2}\mathbf{R}(\gamma_2)$, which are given by

$$
{}^{\mathcal{B}}_{\mathcal{T}_1}\mathbf{R}(\gamma_1) = \begin{bmatrix} \cos(\gamma_1) & 0 & \sin(\gamma_1) \\ 0 & 1 & 0 \\ -\sin(\gamma_1) & 0 & \cos(\gamma_1) \end{bmatrix}, \qquad {}^{\mathcal{B}}_{\mathcal{T}_2}\mathbf{R}(\gamma_2) = \begin{bmatrix} \cos(\gamma_2) & 0 & \sin(\gamma_2) \\ 0 & 1 & 0 \\ -\sin(\gamma_2) & 0 & \cos(\gamma_2) \end{bmatrix}. \tag{4.1}
$$

The inertial, body, and rotor frames are represented graphically in Figure 4.1.

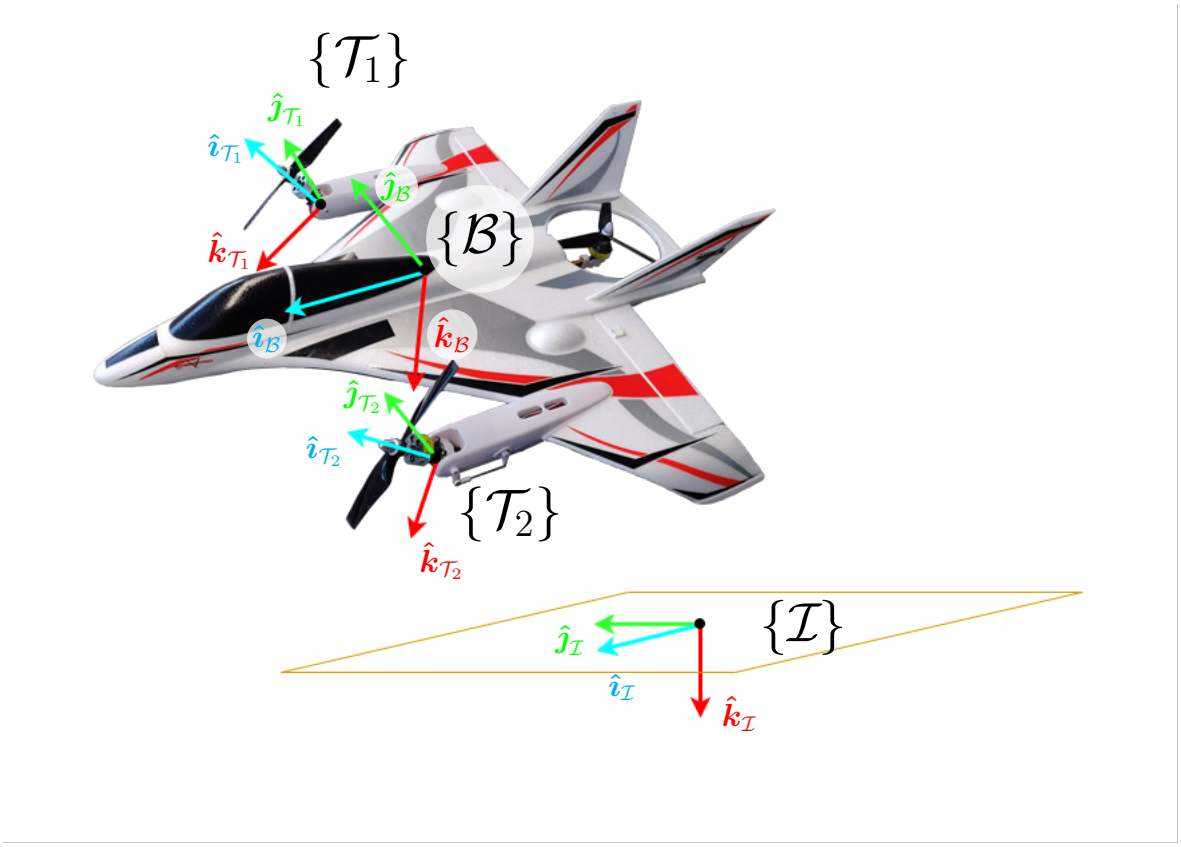

Figure 4.1: Coordinate frames

4.2 Aerodynamic Forces and Moments

As we are dealing with a hybrid UAV, aerodynamic phenomena are significant when the aircraft is in transition or forward flight and, therefore, must be analysed and considered. The aerodynamic forces, $\mathbf{F}_{\text{aero}}$, and moments, $\mathbf{M}_{\text{aero}}$, are divided into two categories: longitudinal and lateral. The model for these forces and moments follows the approach in [28], with some adaptations. The effect of wind is not

considered in this model.

4.2.1 Longitudinal Aerodynamics

Regarding the longitudinal aerodynamics, we start by considering the lift force, $\mathbf{F}_{\text{Lift}}$, and drag force, $\mathbf{F}_{\text{Drag}}$. The magnitude of these forces is, respectively, given by

$$F_{\text{Lift}} = \frac{1}{2}\,\rho\,S\,\left(C_{\text{Lift}}(\alpha) + (1-\sigma(\alpha))\,C_{\text{L},\delta_{\text{e}}}\,\delta_{\text{e}}\right)\,\|^{\mathcal{B}}\mathbf{v}\|^2, \tag{4.2}$$

$$F_{\text{Drag}} = \frac{1}{2}\,\rho\,S\,\left(C_{\text{Drag}}(\alpha) + (1-\sigma(\alpha))\,C_{\text{D},\delta_{\text{e}}}\,\delta_{\text{e}}\right)\,\|^{\mathcal{B}}\mathbf{v}\|^2. \tag{4.3}$$

The forces depend on ρ, the air density, S, the surface area of the UAV, the squared norm of the aircraft's velocity ${}^{\mathcal{B}}\mathbf{v} = \begin{bmatrix} u & v & w \end{bmatrix}^{\mathsf{T}}$ (with respect to the body frame), and on $C_{\text{Lift}}(\alpha)$ and $C_{\text{Drag}}(\alpha)$, the lift and drag coefficients dependent on the aircraft's angle of attack α, respectively, $C_{\text{L},\delta_{\text{e}}}$ and $C_{\text{D},\delta_{\text{e}}}$ the lift and drag (constant) coefficients dependent on the elevators' angle δ_{e}, weighted by $(1-\sigma(\alpha))$, a sigmoid function of the angle of attack which will later be explained. The elevators' angle δ_{e} is given by

$$\delta_{\text{e}} = \delta_{\text{e,r}} + \delta_{\text{e,l}}\,, \tag{4.4}$$

with $\delta_{\text{e,r}}$ and $\delta_{\text{e,l}}$ the right and left elevon deflection angles. The angle of attack is the angle between a reference line in the aircraft (typically in the direction of $\hat{\boldsymbol{\imath}}_{\mathcal{B}}$ of the body frame) and the air velocity vector, and it is given by

$$\alpha = \text{atan2}(w,\,u)\,. \tag{4.5}$$

The lift coefficient, $C_{\text{Lift}}(\alpha)$, is given by

$$C_{\text{Lift}}(\alpha) = (1-\sigma(\alpha))\,\left(C_{\text{Lift},0} + C_{\text{Lift},\alpha}\,\alpha\right) + \sigma(\alpha)\,\left(2\,\text{sign}(\alpha)\,\sin^2(\alpha)\,\cos(\alpha)\right). \tag{4.6}$$

The term $C_{\text{Lift},0}$ is the value of the lift coefficient when the angle of attack is 0, and $C_{\text{Lift},\alpha}$ is a linear coefficient term given by

$$C_{\text{Lift},\alpha} = \frac{\pi\,AR}{1+\sqrt{1+\left(\frac{AR}{2}\right)}}, \tag{4.7}$$

with AR being the aspect ratio of the UAV. The drag coefficient, as a function of the angle of attack, $C_{\text{Drag}}(\alpha)$ is

$$C_{\text{Drag}}(\alpha) = C_{\text{parasitic}} + \frac{(C_{\text{Lift},0} + C_{\text{Lift},\alpha}\,\alpha)^2}{(\pi\,e_{\text{Osw}}\,AR)}, \tag{4.8}$$

with $C_{\text{parasitic}}$ being a coefficient related to parasitic drag, generated by the air moving over the wings, considered constant, and e_{Osw} is the Oswald efficiency factor, related to wing configuration. The function $\sigma(\alpha)$ is a sigmoid function given by

$$\sigma(\alpha) = \frac{1 + e^{-M(\alpha-\alpha_0)} + e^{M(\alpha-\alpha_0)}}{\left(1 + e^{-M(\alpha-\alpha_0)}\right)\ \left(1 + e^{M(\alpha-\alpha_0)}\right)}\ , \tag{4.9}$$

with M and α_0 positive constants. It is mostly used as a weight, adapted from [28], so as to give more importance to aerodynamic phenomena when the angle of attack is smaller than a certain angle α_0, and less importance otherwise, for example in hover, since when the UAV functions in rotary-wing mode, aerodynamics do not have as great an influence as in fixed-wing mode. Plots for the lift and drag coefficients are shown in Figures 4.2 and 4.3, to observe their dependence on the angle of attack. The parameter values used to generate these plots of $C_{\text{Lift}}(\alpha)$ and $C_{\text{Drag}}(\alpha)$ are presented in Appendix A.

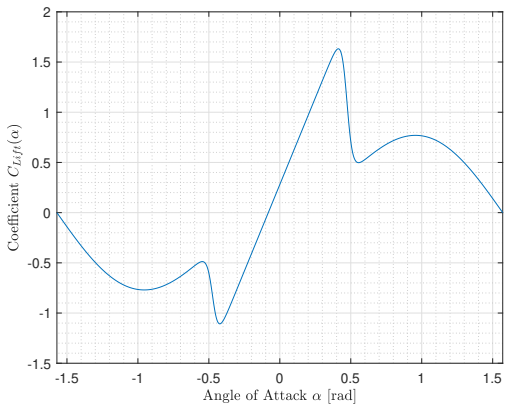

Figure 4.2: Lift coefficient

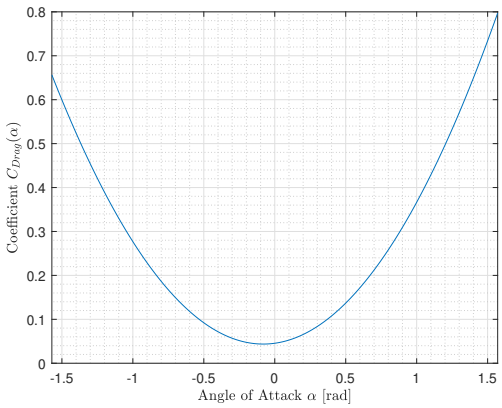

Figure 4.3: Drag coefficient

To get the longitudinal forces in the body frame of the UAV from the lift and drag forces, a rotation by the angle of attack α must be made. As such, the longitudinal aerodynamic force components $F_{\text{aero},i}$ and $F_{\text{aero},k}$ are given by

$$\begin{bmatrix} F_{\text{aero},i} \\ F_{\text{aero},k} \end{bmatrix} = \begin{bmatrix} \cos(\alpha) & -\sin(\alpha) \\ \sin(\alpha) & \cos(\alpha) \end{bmatrix} \begin{bmatrix} -F_{\text{Drag}} \\ -F_{\text{Lift}} \end{bmatrix} . \tag{4.10}$$

In addition to the above forces, there is also a pitching moment $M_{\text{aero},j}$ to be considered, which is given by

$$M_{\text{aero},j} = \frac{1}{2}\, \rho\, S\, c\, (1 - \sigma(\alpha))\ (C_{\text{m}_0} + C_{\text{m}_\alpha}\alpha + C_{\text{m}_\text{e}}\delta_\text{e})\, \|^{\mathcal{B}}\mathbf{v}\|^2 , \tag{4.11}$$

where c is the wing mean chord, C_{m_0} is the value of the pitch coefficient when $\alpha = 0$ and $\delta_\text{e} = 0$, and C_{m_α} is the pitch static stability coefficient. As before, the term $(1 - \sigma(\alpha))$ is present so as to give more importance to these components the closer the hybrid aircraft functions as a fixed-wing aircraft.

4.2.2 Lateral Aerodynamics

The lateral aerodynamics are responsible for lateral translational motion along the direction of $\hat{\boldsymbol{\jmath}}_{\mathcal{B}}$, and for rotational motion in roll and yaw. The lateral force component $F_{\mathrm{aero},j}$, the roll $M_{\mathrm{aero},i}$ and the yaw $M_{\mathrm{aero},k}$ components of $\mathbf{F}_{\mathrm{aero}}$ and $\mathbf{M}_{\mathrm{aero}}$ are given by

$$F_{\mathrm{aero},j} = \frac{1}{2}\,\rho\,S\,(1-\sigma(\alpha))\,\left(C_{\mathrm{Y}_\beta}\beta + C_{\mathrm{Y}_\mathrm{a}}\delta_\mathrm{a}\right)\|^{\mathcal{B}}\mathbf{v}\|^2\,, \tag{4.12}$$

$$M_{\mathrm{aero},i} = \frac{1}{2}\,\rho\,S\,b\,(1-\sigma(\alpha))\left(C_{\mathrm{l}_\beta}\beta + C_{\mathrm{l}_\mathrm{a}}\delta_\mathrm{a}\right)\|^{\mathcal{B}}\mathbf{v}\|^2\,, \tag{4.13}$$

$$M_{\mathrm{aero},k} = \frac{1}{2}\,\rho\,S\,b\,(1-\sigma(\alpha))\left(C_{\mathrm{n}_\beta}\beta + C_{\mathrm{n}_\mathrm{a}}\delta_\mathrm{a}\right)\|^{\mathcal{B}}\mathbf{v}\|^2\,, \tag{4.14}$$

where β is the sideslip angle, b is the UAV wingspan, C_{Y_β} and $C_{\mathrm{Y}_\mathrm{a}}$ are the lateral force coefficient concerning β and δ_a, respectively, C_{l_β} and C_{n_β} are the roll and yaw static stability coefficients, respectively, $C_{\mathrm{l}_\mathrm{a}}$ is the deflection primary control coefficient concerning roll, $C_{\mathrm{n}_\mathrm{a}}$ is the deflection cross-control coefficient concerning yaw. The parameter δ_a is the aileron deflection angle, which is given by

$$\delta_\mathrm{a} = -\,\delta_{\mathrm{e,r}} + \delta_{\mathrm{e,l}}\,, \tag{4.15}$$

in terms of the right and left elevon deflection angles.

4.3 Propulsion Forces and Moments

As mentioned in Chapter 2 the UAV has one tilting rotor over each wing and one fixed rotor on its tail. Let us denote the right and left rotors on the wings by rotor $i = \{1,\ 2\}$, respectively. Each spins with angular velocity ω_i, with rotor 1 spinning anticlockwise and rotor 2 clockwise, and generates a force $\mathbf{F}_i$ and a moment $\mathbf{M}_i$, with magnitudes given by

$$\begin{cases} F_i \;=\; k_\mathrm{F}\,\omega_i^2 - \frac{1}{2}\rho\,S_{\mathrm{rotor}}\|\mathbf{v}_{\mathrm{air,rotor}}\|^2 \\ M_i \;=\; k_\mathrm{M}\,\omega_i^2 \end{cases}\,, \tag{4.16}$$

with k_F and k_M force and moment coefficients related to these rotors, S_{rotor} the rotor surface area, and $\mathbf{v}_{\mathrm{air,rotor}}$ the velocity of the air going into the rotor. The force $\mathbf{F}_i$ is applied in the direction of $\hat{\boldsymbol{\imath}}_{\mathcal{T}_i}$, and the moment $\mathbf{M}_i$ is applied about the axis $\hat{\boldsymbol{\imath}}_{\mathcal{T}_i}$, with opposite signal relative to the angular velocity ω_i. As such, the overall force $\mathbf{F}_{\mathrm{wr}}$ and moment $\mathbf{M}_{\mathrm{wr}}$ from the wing rotors acting on the CoM is given by

$$\begin{aligned}\mathbf{F}_{\mathrm{wr}} &= {}^{\mathcal{B}}_{\mathcal{T}_1}\mathbf{R}\,\mathbf{F}_1 + {}^{\mathcal{B}}_{\mathcal{T}_2}\mathbf{R}\,\mathbf{F}_2 \\ &= \begin{bmatrix} F_1\ \cos(\gamma_1) + F_2\ \cos(\gamma_2) \\ 0 \\ -F_1\sin(\gamma_1) - F_2\sin(\gamma_2) \end{bmatrix}\end{aligned} \qquad \begin{aligned}\mathbf{M}_{\mathrm{wr}} &= {}^{\mathcal{B}}_{\mathcal{T}_1}\mathbf{R}\,\mathbf{M}_1 + {}^{\mathcal{B}}_{\mathcal{T}_2}\mathbf{R}\,\mathbf{M}_2 \\ &= \begin{bmatrix} M_1\ \cos(\gamma_1) - M_2\ \cos(\gamma_2) \\ 0 \\ -M_1\sin(\gamma_2) + M_2\sin(\gamma_2) \end{bmatrix}\end{aligned} \tag{4.17}$$

As a result of not being applied to the CoM of the UAV, $\mathbf{F}_1$ and $\mathbf{F}_2$ generate a moment $\mathbf{M}_{\mathrm{F,wr}}$. Recalling that these forces are applied at positions $\mathbf{r}_1$ and $\mathbf{r}_2$, with respect to the body frame, the moment $\mathbf{M}_{\mathrm{F,wr}}$ is given by

$$\begin{aligned}\mathbf{M}_{\mathrm{F,wr}} &= \mathbf{r}_1 \times \left({}^{\mathcal{B}}_{\mathcal{T}_1}\mathbf{R}\,\mathbf{F}_1\right) + \mathbf{r}_2 \times \left({}^{\mathcal{B}}_{\mathcal{T}_2}\mathbf{R}\,\mathbf{F}_2\right) \\ &= \begin{bmatrix} r_{1,x} \\ r_{1,y} \\ r_{1,z} \end{bmatrix} \times \begin{bmatrix} F_1\cos(\gamma_1) \\ 0 \\ -F_1\sin(\gamma_1) \end{bmatrix} + \begin{bmatrix} r_{2,x} \\ r_{2,y} \\ r_{2,z} \end{bmatrix} \times \begin{bmatrix} F_2\cos(\gamma_2) \\ 0 \\ -F_2\sin(\gamma_2) \end{bmatrix} \\ &= \begin{bmatrix} -r_{1,y}\ F_1\ \sin(\gamma_1) - r_{2,y}\ F_2\ \sin(\gamma_2) \\ r_{1,z}\ F_1\ \cos(\gamma_1) + r_{2,z}\ F_2\ \cos(\gamma_2) + r_{1,x}\ F_1\ \sin(\gamma_1) + r_{2,x}\ F_2\ \sin(\gamma_2) \\ -r_{1,y}\ F_1\ \cos(\gamma_1) - r_{2,y}\ F_2\ \cos(\gamma_2) \end{bmatrix}\end{aligned} \tag{4.18}$$

Besides the force generated by the tilting wing rotors, there is also the force $\mathbf{F}_{\mathrm{tr}}$ and a moment $\mathbf{M}_{\mathrm{tr}}$ from the fixed tail rotor, which spins anticlockwise with angular velocity ω_{tr}. Since this rotor is fixed relative to $\{\mathcal{B}\}$, the force and moment applied to the CoM of the aircraft are simply

$$\begin{aligned}\mathbf{F}_{\mathrm{tr}} &= -F_{\mathrm{tr}}\,\hat{\boldsymbol{k}}_{\mathcal{B}}\,, \\ \mathbf{M}_{\mathrm{tr}} &= M_{\mathrm{tr}}\,\hat{\boldsymbol{k}}_{\mathcal{B}}\,,\end{aligned} \tag{4.19}$$

whose magnitudes are given by

$$\begin{cases} F_{\mathrm{tr}} \ = \ k_{\mathrm{F,tr}}\,\omega_{\mathrm{tr}}^2 \\ M_{\mathrm{tr}} \ = \ k_{\mathrm{M,tr}}\,\omega_{\mathrm{tr}}^2 \end{cases}\,, \tag{4.20}$$

with $k_{\mathrm{F,tr}}$ and $k_{\mathrm{M,tr}}$ the force and moment coefficients for the fixed tail rotor. The air velocity as it enters the tail rotor is not considered, due to its small magnitude. Since $\mathbf{F}_{\mathrm{tr}}$ is not applied directly to the CoM of the UAV, it will generate a pitching moment $\mathbf{M}_{\mathrm{F,tr}}$. Consider the position vector $\mathbf{r}_{\mathrm{tr}}$ with origin in the CoM of the aircraft, with magnitude equal to the distance between the CoM and the point where $\mathbf{F}_{\mathrm{tr}}$ is applied, and pointing to said point. Then, the moment $\mathbf{M}_{\mathrm{F,tr}}$ is

$$\mathbf{M}_{\mathrm{F,tr}} = \mathbf{r}_{\mathrm{tr}} \times \mathbf{F}_{\mathrm{tr}}\,, \tag{4.21}$$

which, assuming that the angle between the position vector and the force vector $\angle(\mathbf{r}_{\mathrm{tr}},\ \mathbf{F}_{\mathrm{tr}}) \approx \frac{\pi}{2}$, yields

$$\mathbf{M}_{\mathrm{F,tr}} = -\|\mathbf{r}_{tr}\|\ k_{\mathrm{F,tr}}\,\omega_{\mathrm{tr}}^2\,\hat{\boldsymbol{\jmath}}_{\mathcal{B}}\,. \tag{4.22}$$

Combining the above expressions, the total force $\mathbf{F}_{\mathrm{rotors}}$ and moment $\mathbf{M}_{\mathrm{rotors}}$ generated by the rotors,

acting on the CoM, are

$$\begin{aligned} \mathbf{F}_{\text{rotors}} &= \mathbf{F}_{\text{wr}} + \mathbf{F}_{\text{tr}} \,, \\ \mathbf{M}_{\text{rotors}} &= \mathbf{M}_{\text{wr}} + \mathbf{M}_{\text{tr}} + \mathbf{M}_{\text{F,wr}} + \mathbf{M}_{\text{F,tr}} \,. \end{aligned} \tag{4.23}$$

4.4 Kinematics and Dynamic Equations

The UAV is modelled as a rigid-body, with forces and moments applied to its CoM. Let the position of the CoM with respect to the inertial frame $\{\mathcal{I}\}$ be denoted by $\mathbf{p} = \begin{bmatrix} p_x & p_y & p_z \end{bmatrix}^{\mathsf{T}}$, and the linear velocity of frame $\{\mathcal{B}\}$ relative to $\{\mathcal{I}\}$, expressed in $\{\mathcal{I}\}$, by $\mathbf{v} = \begin{bmatrix} v_x & v_y & v_z \end{bmatrix}^{\mathsf{T}}$. Further, let $\boldsymbol{q} = (q_0,\, q_1,\, q_2,\, q_3) = (q_0,\, \mathbf{q})$ be the quaternion that represents the UAV's orientation, $\boldsymbol{\omega} = \begin{bmatrix} p & q & r \end{bmatrix}^{\mathsf{T}}$ the UAV's angular velocity and

$$\mathbf{S}_{\text{q}} = \frac{1}{2} \begin{bmatrix} -q_1 & -q_2 & -q_3 \\ q_0 & q_3 & -q_2 \\ -q_3 & q_0 & q_1 \\ q_2 & -q_1 & q_0 \end{bmatrix} \,. \tag{4.24}$$

a transformation matrix defining the rotation rate, with quaternion representation. Thus, the kinematics equations of motion are

$$\dot{\mathbf{p}} = \mathbf{v} \,, \tag{4.25}$$

$$\dot{\boldsymbol{q}} = \mathbf{S}_{\text{q}}\, \boldsymbol{\omega} \,. \tag{4.26}$$

Equation (4.26) may also be expressed as

$$\begin{aligned} \dot{q}_0 &= -\frac{1}{2}\, \mathbf{q}^{\mathsf{T}}\, \boldsymbol{\omega} \\ \dot{\mathbf{q}} &= \frac{1}{2}\, (\mathbf{S}(\mathbf{q}) + q_0\, \mathbf{I}_{3\times 3})\, \boldsymbol{\omega} \end{aligned} \,, \tag{4.27}$$

with $\mathbf{S}(\mathbf{q})$ the skew-symmetric matrix that satisfies $\mathbf{S}(\mathbf{q})\ \mathbf{a} = \mathbf{q} \times \mathbf{a}$, for any vector $\mathbf{a} \in \mathbb{R}^3$ and $\mathbf{I}_{3\times 3}$ the 3×3 identity matrix [22].

In addition, acting on the CoM are also the force due to gravity $\mathbf{F}_{\text{g}} = \begin{bmatrix} 0 & 0 & m\, g \end{bmatrix}^{\mathsf{T}}$, with m being the UAV's mass and $g = 9.8\,\text{m/s}^2$, the aerodynamic forces and moments, $\mathbf{F}_{\text{aero}}$ and $\mathbf{M}_{\text{aero}}$, and rotor forces and moments, $\mathbf{F}_{\text{rotors}}$ and $\mathbf{M}_{\text{rotors}}$. Hence, the Newton-Euler equations of motion are

$$m\dot{\mathbf{v}} = \mathbf{F}_{\text{g}} + {}^{\mathcal{I}}_{\mathcal{B}}\mathbf{R}\, \mathbf{F}_{\text{aero}} + {}^{\mathcal{I}}_{\mathcal{B}}\mathbf{R}\, \mathbf{F}_{\text{rotors}} \,, \tag{4.28}$$

$$\mathbf{J}\, \dot{\boldsymbol{\omega}} = -\mathbf{S}(\boldsymbol{\omega})\, \mathbf{J}\, \boldsymbol{\omega} + \mathbf{M}_{\text{aero}} + \mathbf{M}_{\text{rotors}} \,, \tag{4.29}$$

with $\mathbf{J}$ being the inertia matrix of the UAV and ${}^{\mathcal{I}}_{\mathcal{B}}\mathbf{R}$ the rotation matrix from the body-fixed frame $\{\mathcal{B}\}$ to the inertial frame $\{\mathcal{I}\}$. By analysing the aerodynamic force and moment, $\mathbf{F}_{\text{aero}}$ and $\mathbf{M}_{\text{aero}}$, and the rotors force and moment, $\mathbf{F}_{\text{rotors}}$ and $\mathbf{M}_{\text{rotors}}$, it is noted that, in the absence of wind, these may be

decomposed into forces and moments that depend solely on the state (more precisely the velocity) of the UAV, $\mathbf{F}_{\text{state}}(\mathbf{v})$ and $\mathbf{M}_{\text{state}}(\mathbf{v})$, and on the states and inputs, $\mathbf{F}_{\text{inputs}}(\mathbf{v},\,\mathbf{u})$ and $\mathbf{M}_{\text{inputs}}(\mathbf{v},\,\mathbf{u})$, with inputs $\mathbf{u} = \begin{bmatrix}\omega_1 & \omega_2 & \omega_{\text{tr}} & \gamma_1 & \gamma_2 & \delta_{\text{e,l}} & \delta_{\text{e,r}}\end{bmatrix}$. Thus, (4.28) and (4.29) may be rewritten as

$$m\dot{\mathbf{v}} = \mathbf{F}_{\text{g}} + {}^{\mathcal{I}}_{\mathcal{B}}\mathbf{R}\left(\mathbf{F}_{\text{state}} + \mathbf{F}_{\text{inputs}}\right)\ , \tag{4.30}$$

$$\mathbf{J}\,\dot{\boldsymbol{\omega}} = -\mathbf{S}(\boldsymbol{\omega})\,\mathbf{J}\,\boldsymbol{\omega} + \mathbf{M}_{\text{state}} + \mathbf{M}_{\text{inputs}}\ . \tag{4.31}$$

This rearrangement will be useful in the control strategy deduced in Chapter 5.

4.5 Error Dynamics

The system error dynamics will be of importance when deriving the control strategy. To begin, the position error $\widetilde{\mathbf{p}}$ is defined to be the difference between the position and its reference. Similarly, its time-derivative, the velocity error $\widetilde{\mathbf{v}}$ is defined as the difference between the velocity and its reference. As such, these two terms are given by

$$\widetilde{\mathbf{p}} = \mathbf{p} - \mathbf{p}_{\text{ref}}\ , \tag{4.32}$$

$$\widetilde{\mathbf{v}} = \dot{\widetilde{\mathbf{p}}} = \mathbf{v} - \mathbf{v}_{\text{ref}}\ . \tag{4.33}$$

The time-derivative of the velocity error, the acceleration error $\widetilde{\mathbf{a}}$, is thus given by

$$\dot{\widetilde{\mathbf{v}}} = \widetilde{\mathbf{a}} = \mathbf{g} + \frac{1}{m}\,{}^{\mathcal{I}}_{\mathcal{B}}\mathbf{R}\,\mathbf{F}_{\text{states}} + \frac{1}{m}\,{}^{\mathcal{I}}_{\mathcal{B}}\mathbf{R}\,\mathbf{F}_{\text{inputs}} - \mathbf{a}_{\text{ref}} \tag{4.34}$$

Regarding attitude, the orientation error $\widetilde{\boldsymbol{q}}$ is defined as the quaternion product of the orientation reference conjugate by the orientation of the UAV

$$\widetilde{\boldsymbol{q}} = (\widetilde{q}_0,\,\widetilde{\mathbf{q}}) = \bar{\boldsymbol{q}}_{\text{ref}} \circ \boldsymbol{q} \tag{4.35}$$

From (3.12) and (4.35), the error rotation matrix $\widetilde{\mathbf{R}}$ that corresponds to the above orientation error quaternion representation is defined as

$$\widetilde{\mathbf{R}} = \mathbf{R}(\widetilde{\boldsymbol{q}})\,. \tag{4.36}$$

Finally, the angular velocity error $\widetilde{\boldsymbol{\omega}}$ is given by

$$\widetilde{\boldsymbol{\omega}} = \boldsymbol{\omega} - \widetilde{\mathbf{R}}\,\boldsymbol{\omega}_{\text{ref}} \tag{4.37}$$

and its time-derivative, the angular acceleration error, is given by

$$\begin{aligned}\dot{\widetilde{\boldsymbol{\omega}}} &= \dot{\boldsymbol{\omega}} - \frac{d}{dt}\left(\widetilde{\mathbf{R}}\,\boldsymbol{\omega}_{\mathrm{ref}}\right) \\ &= \mathbf{J}^{-1}\left(-\mathbf{S}(\boldsymbol{\omega})\,\mathbf{J}\,\boldsymbol{\omega} + \mathbf{M}_{\mathrm{states}} + \mathbf{M}_{\mathrm{inputs}}\right) - \left(\widetilde{\mathbf{R}}\,\dot{\boldsymbol{\omega}}_{\mathrm{ref}} - \mathbf{S}(\widetilde{\boldsymbol{\omega}})\,\widetilde{\mathbf{R}}\,\boldsymbol{\omega}_{\mathrm{ref}}\right) .\end{aligned} \tag{4.38}$$

5

Control

Contents

This chapter presents the control strategy for the trajectory tracking problem. First, the overall control scheme is described. Then, we deal with the issues of position and attitude control, based on backstepping procedures that generate force and moment references. Finally, the control allocation problem is divided into two parts, concerning longitudinal and lateral allocation of the reference forces and moments, and addressed using nonlinear optimisation techniques.

5.1 Control System Architecture

Tiltrotor UAVs are nonlinear systems with coupled dynamics. These characteristics represent a challenge when it comes to devising control strategies. Fixed-wing and rotary-wing UAVs both generate thrust in a fixed direction relative to the body frame, which means that if one wants to generate force in a certain direction of the inertial frame, the required orientation of the vehicle can be calculated with relative ease and, therefore, cascade control solutions are standard practice for these vehicles. In this type of control structure, an outer loop deals with position control and feeds an inner control loop which deals with attitude control.

Such an architecture is not as straightforward for tiltrotor UAVs, since the generated thrust direction can be changed by adjusting the tilt angle of the rotors. This means that, given a certain thrust reference, the required attitude of the vehicle is not determined. For example, to have the vehicle hover, the generated force must be directed upwards in order to counteract the force of gravity, which can be achieved by having the UAV in a levelled position, with roll and pitch angles equal to zero, and rotors tilted upwards, or with the UAV at a 90° pitch angle, with rotors tilted forwards at 0°. Comparing these two solutions to the same problem, and taking into account the way the vehicle is intended to work, one concludes that the former is more advisable than the latter. Despite this additional difficulty, a cascaded control architecture is nonetheless appropriate due to the coupled dynamics of the system at hand. An explanation of how an attitude reference is calculated is provided in the following section.

The overall control system architecture diagram is presented in Figure 5.1. The Trajectory Handler provides the trajectory references (position $\mathbf{p}_{\text{ref}}$, velocity $\mathbf{v}_{\text{ref}}$, and acceleration $\mathbf{a}_{\text{ref}}$) to the Controller, which calculates force $\mathbf{F}_{\text{ref}}$ and moment $\mathbf{M}_{\text{ref}}$ necessary to achieve the received trajectory reference.The Controller is divided into two blocks. The first block is the Position Controller, which receives the trajectory reference and the UAV state and computes the force reference $\mathbf{F}_{\text{ref}}$, the orientation quaternion reference $\boldsymbol{q}_{\text{ref}}$, and the angular velocity reference $\boldsymbol{\omega}_{\text{ref}}$. Both $\boldsymbol{q}_{\text{ref}}$ and $\boldsymbol{\omega}_{\text{ref}}$ are transmitted to the second block, the Attitude Controller, which calculates the moment reference $\mathbf{M}_{\text{ref}}$. The Controller architecture is shown in Figure 5.2. The Control Allocation block computes the input values $\mathbf{u}$ that generate the force and moment references, which are then fed into the tiltrotor UAV model.

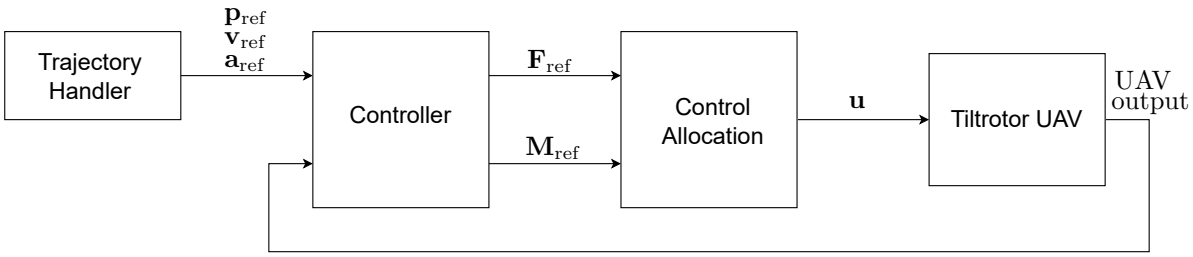

Figure 5.1: Control System Architecture

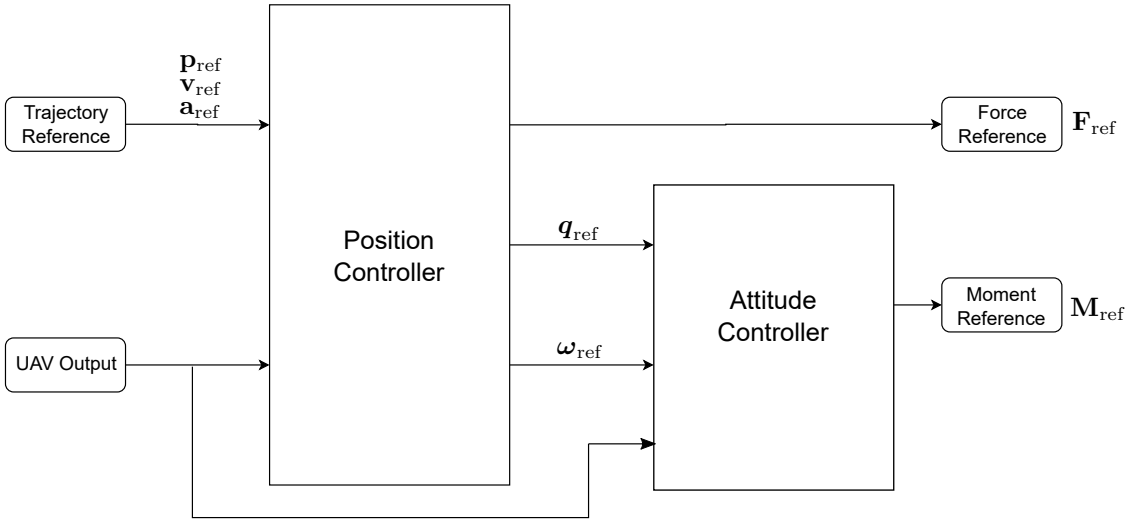

Figure 5.2: Controller Architecture

5.2 Position and Attitude Control via Backstepping

The approach to position and attitude control is similar to the one in [30]. The force and moment references, $\mathbf{F}_{\text{ref}}$ and $\mathbf{M}_{\text{ref}}$, that are fed into the Control Allocation block are generated via backstepping.

5.2.1 Position Control

Regarding the position control, the objective is to have the UAV closely follow the trajectory reference, or in other words, to drive the error between the real and reference trajectories to zero. To this effect, we make use of the error dynamics model introduced in Chapter 4. To drive error dynamics related to linear motion, presented in Equations (4.32) and (4.33), to zero, we first define the system

$$\begin{aligned} \boldsymbol{\xi}_1 &= \tilde{\mathbf{p}} \\ \boldsymbol{\xi}_2 &= \tilde{\mathbf{v}} - \boldsymbol{\alpha}_1(\boldsymbol{\xi}_1) \end{aligned} \quad , \tag{5.1}$$

with $\boldsymbol{\alpha}_1(\boldsymbol{\xi}_1)$ being the virtual controller to be calculated. To begin the backstepping procedure, as explained in Chapter 3, a candidate Lyapunov function designated by V_1 is proposed. A common choice are quadratic functions [24]. As such, V_1 is defined as

$$V_1 = \frac{1}{2}\,\boldsymbol{\xi}_1^{\mathsf{T}}\,\boldsymbol{\xi}_1 + \frac{1}{2}k_{1,\mathrm{I}}\left[\int \boldsymbol{\xi}_1 dt\right]^{\mathsf{T}}\left[\int \boldsymbol{\xi}_1 dt\right] . \tag{5.2}$$

This Lyapunov function is quadratic in the position error $\boldsymbol{\xi}_1$ and in the integral of the position error. The function includes a term related to the integral of the position error, as it will play a role in the controller, adding integral action to provide improved trajectory following. Taking the derivative of V_1, which should satisfy the condition $\dot{V}_1 \leq 0$, it follows that

$$\begin{aligned} \dot{V}_1 &= \boldsymbol{\xi}_1^{\mathsf{T}}\,\dot{\boldsymbol{\xi}}_1 + k_{1,\mathrm{I}}\,\left[\int \boldsymbol{\xi}_1 dt\right]^{\mathsf{T}}\left[\int \dot{\boldsymbol{\xi}}_1 dt\right] \\ &= \boldsymbol{\xi}_1^{\mathsf{T}}\,(\boldsymbol{\xi}_2 \;+\; \boldsymbol{\alpha}_1(\boldsymbol{\xi}_1)) + k_{1,\mathrm{I}}\,\left[\int \boldsymbol{\xi}_1 dt\right]^{\mathsf{T}}\boldsymbol{\xi}_1 \end{aligned} \tag{5.3}$$

Taking the virtual controller $\boldsymbol{\alpha}_1$ to be

$$\boldsymbol{\alpha}_1(\boldsymbol{\xi}_1) = -k_1\,\boldsymbol{\xi}_1 - k_{1,\mathrm{I}}\left[\int \boldsymbol{\xi}_1 dt\right] , \tag{5.4}$$

with constants $k_1 > 0$ and $k_{1,\mathrm{I}} > 0$, it follows that the derivative $\dot{V}_1$ is given by

$$\begin{aligned} \dot{V}_1 &= -k_1\,\boldsymbol{\xi}_1^{\mathsf{T}}\,\boldsymbol{\xi}_1 \;+\; \boldsymbol{\xi}_1^{\mathsf{T}}\,\boldsymbol{\xi}_2 \;-\; k_{1,\mathrm{I}}\,\boldsymbol{\xi}_1^{\mathsf{T}}\left[\int \boldsymbol{\xi}_1 dt\right] \;+\; k_{1,\mathrm{I}}\left[\int \boldsymbol{\xi}_1 dt\right]^{\mathsf{T}}\boldsymbol{\xi}_1 \\ &= -k_1\,\|\,\boldsymbol{\xi}_1\|^2 \;+\; \boldsymbol{\xi}_1^{\mathsf{T}}\,\boldsymbol{\xi}_2\,. \end{aligned} \tag{5.5}$$

Since the goal is to have $\dot{V}_1 \leq 0$, from (5.5), one concludes that, as $-k_1 \, \| \boldsymbol{\xi}_1 \|^2 \leq 0$, such is only possible if $\boldsymbol{\xi}_2 = \mathbf{0}$. This would imply that $\boldsymbol{\xi}_1$, the position error, converged to zero as intended. To achieve this objective, we build upon V_1 by defining a second candidate Lyapunov function designated V_2 as

$$V_2 = V_1 + \frac{1}{2} \, \boldsymbol{\xi}_2^{\mathsf{T}} \, \boldsymbol{\xi}_2 \, , \tag{5.6}$$

which incorporates the previous Lyapunov function and adds a quadratic term of the velocity error $\boldsymbol{\xi}_2$. As before, the following step is to compute the derivative of V_2, which is

$$\begin{aligned} \dot{V}_2 &= \dot{V}_1 + \boldsymbol{\xi}_2^{\mathsf{T}} \left(\dot{\tilde{\mathbf{v}}} \; + \; k_1 \, \dot{\boldsymbol{\xi}}_1 \; + \; k_{1,\mathrm{I}} \, \boldsymbol{\xi}_1 \right) \\ &= -k_1 \, \| \boldsymbol{\xi}_1 \|^2 + \boldsymbol{\xi}_1^{\mathsf{T}} \, \boldsymbol{\xi}_2 + \boldsymbol{\xi}_2^{\mathsf{T}} \left(\mathbf{g} + \frac{1}{m} \mathbf{F}_{\mathrm{state}} + \frac{1}{m} \mathbf{F}_{\mathrm{input}} - \dot{\mathbf{v}}_{\mathrm{ref}} + k_1 \, (\boldsymbol{\xi}_2 + \boldsymbol{\alpha}_1(\boldsymbol{\xi}_1)) \; + \; k_{1,\mathrm{I}} \, \boldsymbol{\xi}_1 \right) \\ &= -k_1 \, \| \boldsymbol{\xi}_1 \|^2 + \boldsymbol{\xi}_1^{\mathsf{T}} \, \boldsymbol{\xi}_2 + \boldsymbol{\xi}_2^{\mathsf{T}} \left(\mathbf{g} + \frac{1}{m} \mathbf{F}_{\mathrm{state}} + \frac{1}{m} \mathbf{F}_{\mathrm{input}} - \mathbf{a}_{\mathrm{ref}} + k_1 \, \boldsymbol{\xi}_2 + (k_{1,\mathrm{I}} - k_1^2) \, \boldsymbol{\xi}_1 \right. \\ &\qquad \left. - k_1 \, k_{1,\mathrm{I}} \left[\int \boldsymbol{\xi}_1 dt \right] \right) \, . \end{aligned} \tag{5.7}$$

Note that in (5.7), the notation $\mathbf{F}_{\mathrm{state}}$ and $\mathbf{F}_{\mathrm{input}}$ is used, since the purpose of this procedure is to find a force reference that will be generated by the Control Allocation block, i.e. by the actuators of the UAV. Once again, to guarantee stability, or more explicitly the convergence of the position and velocity errors to zero, it is necessary that $\dot{V}_2 \leq 0$. Therefore, the next step is to calculate the expression for $\mathbf{F}_{\mathrm{input}}$ that will achieve this goal. Defining $\mathbf{F}_{\mathrm{ref}}$ as the $\mathbf{F}_{\mathrm{input}}$ that stabilises the system, the derivation of the expression gives

$$\begin{aligned} \mathbf{F}_{\mathrm{ref}} &= m \left(-\mathbf{g} - \frac{1}{m} \mathbf{F}_{\mathrm{state}} + \mathbf{a}_{\mathrm{ref}} - k_1 \, \boldsymbol{\xi}_2 - (k_{1,\mathrm{I}} - k_1^2) \, \boldsymbol{\xi}_1 + k_1 \, k_{1,\mathrm{I}} \left[\int \boldsymbol{\xi}_1 dt \right] - \boldsymbol{\xi}_1 - k_2 \, \boldsymbol{\xi}_2 \right) \\ &= m \left(-\mathbf{g} - \frac{1}{m} \mathbf{F}_{\mathrm{state}} + \mathbf{a}_{\mathrm{ref}} - (1 + k_{1,\mathrm{I}} - k_1^2) \, \boldsymbol{\xi}_1 + k_1 \, k_{1,\mathrm{I}} \left[\int \boldsymbol{\xi}_1 dt \right] \right. \\ &\qquad \left. - (k_1 + k_2) \, \left(\tilde{\mathbf{v}} \; + \; k_1 \, \boldsymbol{\xi}_1 + k_{1,\mathrm{I}} \left[\int \boldsymbol{\xi}_1 dt \right] \right) \right) \\ &= m \left(-\mathbf{g} - \frac{1}{m} \mathbf{F}_{\mathrm{state}} + \mathbf{a}_{\mathrm{ref}} - (k_1 + k_2) \, \tilde{\mathbf{v}} - (1 + k_{1,\mathrm{I}} + k_1 k_2) \, \tilde{\mathbf{p}} - k_{1,\mathrm{I}} k_2 \left[\int \tilde{\mathbf{p}} \, dt \right] \right) \\ &= -\mathbf{F}_{\mathrm{g}} - \mathbf{F}_{\mathrm{state}} + m \left(\; \mathbf{a}_{\mathrm{ref}} - (k_1 + k_2) \, \tilde{\mathbf{v}} - (1 + k_{1,\mathrm{I}} + k_1 k_2) \, \tilde{\mathbf{p}} - k_{1,\mathrm{I}} k_2 \left[\int \tilde{\mathbf{p}} \, dt \right] \right) \quad , \end{aligned} \tag{5.8}$$

with $k_2 > 0$. This expression cancels out most of the terms in (5.7), leaving $\dot{V}_2$ with only negative terms of the position and velocity errors. This implies

$$\dot{V}_2 = -k_1 \, \| \boldsymbol{\xi}_1 \|^2 - k_2 \, \| \boldsymbol{\xi}_2 \|^2 \leq 0 \, , \tag{5.9}$$

which was the intended objective. Thus, with force reference $\mathbf{F}_{\mathrm{ref}}$, both the position and velocity errors

converge to $\mathbf{0}$.

It is also the role of the position controller to derive the orientation and angular velocity references that are transmitted to the attitude controller. As explained before, in aircraft with fixed rotors, having calculated the force reference, the required orientation can be readily determined. As this is not the case for tiltrotor UAVs, a more elaborate method must be taken. The approach involves an optimisation problem and is similar to the one described and implemented in [20].

The main difficulty in finding the required attitude stems from the additional degree of freedom that the tilting rotors provide. Hence, the first step taken is to find an estimate of the tilt angle at which the rotors should be, which fixes the generated force from the front rotors in a certain direction. However, even with a determined tilt angle, the attitude problem is not solved, because the front rotors generate force in a different direction than the back rotor (unless the tilt rotors point directly upwards). Nonetheless, fixing a tilt angle reduces the complexity of the problem and, therefore, to calculate the estimated values some assumptions are made. We assume that the estimated tilt angle is the same for both rotors and that the resulting pitching moment should be zero. As a consequence, the tilt angle estimate γ_{est} that will be considered is given by

$$\gamma_{\text{est}} = \text{sat}\left(\text{atan2}\left(F_{\text{ref},k}\ ,\ F_{\text{ref},i}\left(1+\frac{r_{1,x}}{r_{\text{tr},x}}\right)\right)\right)\ , \tag{5.10}$$

which is limited by a saturation function between $\gamma_{\min}$ and $\gamma_{\max}$, the minimum and maximum values of the tilt angle.

Note that the force reference $\mathbf{F}_{\text{ref}}$ derived in (5.8) is defined in the inertial frame. However, the force reference used in (5.10) refers to the body frame, taking into consideration the current aircraft attitude. This might seem counter-intuitive, as the objective is to find the desired attitude necessary to generate the force reference. Considering that the rotors tilt in a pitching motion, the current pitch of the UAV will influence the tilt angle estimate, while the roll and yaw will not. Be that as it may, the normal functioning of tiltrotor aircraft is characterised by a small pitch angle in any flight mode, so this issue is dealt with in the following step.

Despite simplifying the attitude reference calculation by setting a tilt angle estimate, it is still complex. To determine the attitude, the problem is formulated as the following optimisation problem:

$$\underset{\phi,\,\theta,\,\psi,F_1,\,F_2,\,F_{\text{tr}}}{\text{minimise}} \quad \left\|{}^{\mathcal{I}}_{\mathcal{B}}\mathbf{R}(\phi,\,\theta,\,\psi)\,\mathbf{F}_{\text{rotors}}(F_1,\,F_2,\,F_{\text{tr}},\gamma_{\text{est}}) - \mathbf{F}_{\text{ref}}\right\|_2 \tag{5.11}$$

$$\begin{aligned}
\text{subject to} \quad & 0 \leq F_1 \\
& 0 \leq F_2 \\
& 0 \leq F_{\text{tr}} \\
& -\tfrac{\pi}{2} \leq \phi \leq \tfrac{\pi}{2} \\
& \theta_{\min} \leq \theta \leq \theta_{\max} \\
& -\pi \leq \psi \leq \pi
\end{aligned}$$

The variables are the roll, pitch and yaw angles, as well as the forces generated by each rotor. The objective is to minimise the difference between the reference force and the force generated by rotors in a desired attitude encoded by the rotation matrix ${}^{\mathcal{I}}_{\mathcal{B}}\mathbf{R}(\phi,\, \theta,\, \psi)$. The issue of the interference between the aircraft's pitch and the tilt angle is addressed by limiting the pitch angle to the interval $[\theta_{\min},\, \theta_{\max}]$, which limits the effects of situations with large pitch angles, which should not occur. The results presented in Chapter 6 are obtained assuming $\theta_{\min} = -10^{\circ}$ and $\theta_{\max} = 10^{\circ}$.

Denoting the rotation matrix that results from (5.11) by ${}^{\mathcal{I}}_{\mathcal{B}}\mathbf{R}_{\text{ref}}$, using the properties explained in Chapter 3, the corresponding reference quaternion $\boldsymbol{q}_{\text{ref}}$ can be calculated and passed on to the attitude controller. The reason that problem (5.11) used roll, pitch and yaw angles instead of quaternions is that it reduces the complexity, as quaternions have four elements that would need to be calculated, and it simplified the approach to limit the pitch angle.

Having an orientation reference in quaternion form, the procedure to compute the angular velocity reference $\boldsymbol{\omega}_{\text{ref}}$ is similar to the one in [17], in which $\boldsymbol{\omega}_{\text{ref}}$ is proportional to the vector part of the quaternion that results from the multiplication of the reference orientation quaternion $\boldsymbol{q}_{\text{ref}}$ and the current orientation quaternion $\boldsymbol{q}$. Since quaternion multiplication may be interpreted as the error between two quaternions, as the vector part of the multiplication of a quaternion by itself is $\mathbf{0}$, as seen in Chapter 3, this means that $\boldsymbol{\omega}_{\text{ref}}$ is simply proportional to the orientation error. Therefore, the angular velocity reference is given by

$$\boldsymbol{\omega}_{\text{ref}} = k_{\omega}\ \text{vec}\left(\bar{\boldsymbol{q}}_{\text{ref}} \circ \boldsymbol{q}\right)\ , \tag{5.12}$$

where $k_{\omega} > 0$ is a constant and $\text{vec}(\cdot)$ is a function that returns the vector part of a quaternion. Both $\boldsymbol{q}_{\text{ref}}$ and $\boldsymbol{\omega}_{\text{ref}}$ are passed on to the attitude controller.

5.2.2 Attitude Control

Regarding the attitude control, the strategy is similar to the one described above. The goal is to drive the error between the real attitude and the reference that is passed on from the position controller to zero, so that the UAV follows the attitude reference. Making use of the error dynamics model related to angular motion, presented in Equations (4.35) - (4.37), we define the system

$$\begin{aligned} \boldsymbol{\xi}_3 &= \widetilde{\mathbf{q}} \\ \boldsymbol{\xi}_4 &= \widetilde{\boldsymbol{\omega}} - \boldsymbol{\alpha}_2(\boldsymbol{\xi}_3) \end{aligned}\ , \tag{5.13}$$

with virtual controller $\boldsymbol{\alpha}_2(\boldsymbol{\xi}_3)$ to be derived. As in the previous case, we propose a candidate Lyapunov function designated by V_3 that is defined as

$$V_3 = \frac{1}{2}\, \boldsymbol{\xi}_3^{\mathsf{T}}\, \boldsymbol{\xi}_3\,. \tag{5.14}$$

This Lyapunov function is quadratic in the orientation error $\boldsymbol{\xi}_3$. Taking the derivative of V_3, which should satisfy the condition $\dot{V}_3 \leq 0$, we have

$$\begin{aligned}
\dot{V}_3 &= \boldsymbol{\xi}_3^{\mathsf{T}}\, \dot{\boldsymbol{\xi}}_3 \\
&= \boldsymbol{\xi}_3^{\mathsf{T}}\, \dot{\tilde{\mathbf{q}}} \\
&= \frac{1}{2}\, \boldsymbol{\xi}_3^{\mathsf{T}} \left(\mathbf{S}(\boldsymbol{\xi}_3) \;+\; \underbrace{\sqrt{1 - \boldsymbol{\xi}_3^{\mathsf{T}} \boldsymbol{\xi}_3}}_{\widetilde{q}_0}\, \mathbf{I}_{3\times 3} \right) \widetilde{\boldsymbol{\omega}} \\
&= \frac{1}{2}\, \boldsymbol{\xi}_3^{\mathsf{T}} \left(\mathbf{S}(\boldsymbol{\xi}_3) \;+\; \sqrt{1 - \boldsymbol{\xi}_3^{\mathsf{T}} \boldsymbol{\xi}_3}\, \mathbf{I}_{3\times 3} \right) \left(\boldsymbol{\xi}_4 + \boldsymbol{\alpha}_2(\boldsymbol{\xi}_3) \right) .
\end{aligned} \tag{5.15}$$

For convenience, let us denote $\widetilde{\mathbf{Q}} = \left(\mathbf{S}(\boldsymbol{\xi}_3) \;+\; \sqrt{1 - \boldsymbol{\xi}_3^{\mathsf{T}} \boldsymbol{\xi}_3}\, \mathbf{I}_{3\times 3} \right)$. Note that since $\widetilde{\boldsymbol{q}}$ is a unit quaternion, then $\widetilde{q}_0 = \sqrt{1 - \boldsymbol{\xi}_3^{\mathsf{T}} \boldsymbol{\xi}_3}$. By analysing (5.15) with the purpose of making $\dot{V}_3$ have a negative term related to the norm of the orientation error $\|\boldsymbol{\xi}_3\|$, we construct the virtual controller as

$$\boldsymbol{\alpha}_2(\boldsymbol{\xi}_3) = -2\, k_3\, \widetilde{\mathbf{Q}}^{-1}\, \boldsymbol{\xi}_3 \,, \tag{5.16}$$

with constant $k_3 > 0$, which accomplishes this goal. This can be verified by substituting (5.16) into (5.15), which results in

$$\dot{V}_3 = -k_3\, \|\, \boldsymbol{\xi}_3\|^2 + \frac{1}{2}\, \boldsymbol{\xi}_3^{\mathsf{T}}\, \widetilde{\mathbf{Q}}\, \boldsymbol{\xi}_4 \,. \tag{5.17}$$

Thus, as $\dot{V}_3$ has a negative term $-k_3\, \|\, \boldsymbol{\xi}_3\|^2 \leq 0$, and since the objective is that $\dot{V}_3 \leq 0$, one concludes that such is possible provided $\widetilde{\mathbf{Q}}\, \boldsymbol{\xi}_4 \;=\; \mathbf{0}$, meaning that the orientation error $\boldsymbol{\xi}_3$ would go to zero as intended. For this reason, we define a second candidate Lyapunov function designated V_4 as

$$V_4 = V_3 + \frac{1}{2}\, \boldsymbol{\xi}_4^{\mathsf{T}}\, \boldsymbol{\xi}_4 \tag{5.18}$$

which complements V_3 by including a quadratic term of the angular velocity error. The derivative of this Lyapunov function V_4 is

$$\begin{aligned}
\dot{V}_4 &= \dot{V}_3 + \boldsymbol{\xi}_4^{\mathsf{T}}\, \dot{\boldsymbol{\xi}}_4 \\
&= \dot{V}_3 + \boldsymbol{\xi}_4^{\mathsf{T}} \left(\dot{\widetilde{\boldsymbol{\omega}}} - \dot{\boldsymbol{\alpha}}_2(\boldsymbol{\xi}_3) \right) \\
&= -k_3\, \|\, \boldsymbol{\xi}_3\|^2 + \frac{1}{2}\, \boldsymbol{\xi}_3^{\mathsf{T}}\, \widetilde{\mathbf{Q}}\, \boldsymbol{\xi}_4 + \\
&+ \boldsymbol{\xi}_4^{\mathsf{T}} \left(\mathbf{J}^{-1} \left(-\mathbf{S}(\boldsymbol{\omega})\, \mathbf{J}\, \boldsymbol{\omega} + \mathbf{M}_{\text{state}} + \mathbf{M}_{\text{input}} \right) - \left(\widetilde{\mathbf{R}}\, \dot{\boldsymbol{\omega}}_{\text{ref}} - \mathbf{S}(\widetilde{\boldsymbol{\omega}})\, \widetilde{\mathbf{R}}\, \boldsymbol{\omega}_{\text{ref}} \right) - \dot{\boldsymbol{\alpha}}_2(\boldsymbol{\xi}_3) \right)
\end{aligned} \tag{5.19}$$

As previously, the notation $\mathbf{M}_{\text{state}}$ and $\mathbf{M}_{\text{input}}$ is used in (5.19), as it is more practical to find a moment reference to be generated by the Control Allocation block. To guarantee the convergence of the orientation and angular velocity errors to zero, it is required that $\dot{V}_4 \leq 0$. As such, one must derive the

expression for $\mathbf{M}_{\text{input}}$ that will achieve stability. Defining $\mathbf{M}_{\text{ref}}$ as the $\mathbf{M}_{\text{input}}$ that accomplishes this, the expression is given by

$$\mathbf{M}_{\text{ref}} = \mathbf{S}(\boldsymbol{\omega})\mathbf{J}\,\boldsymbol{\omega} \;-\; \mathbf{M}_{\text{state}} + \mathbf{J}\left(\widetilde{\mathbf{R}}\,\dot{\boldsymbol{\omega}}_{\text{ref}} - \mathbf{S}(\boldsymbol{\omega})\,\widetilde{\mathbf{R}}\,\boldsymbol{\omega}_{\text{ref}} + \dot{\boldsymbol{\alpha}}_2(\boldsymbol{\xi}_3) - k_4\,\boldsymbol{\xi}_4 - \frac{1}{2}\,\widetilde{\mathbf{Q}}^{\mathsf{T}}\,\boldsymbol{\xi}_3\right)\,, \tag{5.20}$$

where $k_4 > 0$ is a constant. The derivative of the virtual controller $\dot{\boldsymbol{\alpha}}_2(\boldsymbol{\xi}_3)$ is given by

$$\begin{aligned}\dot{\boldsymbol{\alpha}}_2(\boldsymbol{\xi}_3) &= -2\,k_3\,\left[\left(\dot{\widetilde{\mathbf{Q}}^{-1}}\right)\boldsymbol{\xi}_3 \;+\; \widetilde{\mathbf{Q}}^{-1}\,\dot{\boldsymbol{\xi}}_3\right] \\ &= -2\,k_3\,\left[-\,\widetilde{\mathbf{Q}}^{-1}\,\dot{\widetilde{\mathbf{Q}}}\,\widetilde{\mathbf{Q}}^{-1}\,\boldsymbol{\xi}_3 \;+\; \widetilde{\mathbf{Q}}^{-1}\,\dot{\boldsymbol{\xi}}_3\right] \\ &= -2\,k_3\,\left[-\,\widetilde{\mathbf{Q}}^{-1}\,\dot{\widetilde{\mathbf{Q}}}\,\widetilde{\mathbf{Q}}^{-1}\,\boldsymbol{\xi}_3 \;+\; \frac{1}{2}\,\widetilde{\boldsymbol{\omega}}\right]\,.\end{aligned} \tag{5.21}$$

Substituting (5.20) and (5.21) in (5.19), most terms are cancelled out, leaving $\dot{V}_4$ with only negative terms of the orientation and angular velocity errors, i.e.

$$\dot{V}_4 = -k_3\,\|\,\boldsymbol{\xi}_3\|^2 - k_4\,\|\,\boldsymbol{\xi}_4\|^2 \leq 0\,, \tag{5.22}$$

which was the objective. As such, with moment reference $\mathbf{M}_{\text{ref}}$, both the orientation and angular velocity errors converge to $\mathbf{0}$.

5.3 Control Allocation

The control allocation issue is complex, particularly considering a unified approach to the control of hybrid UAVs, once again because the direction of the generated forces and moments can be changed. In the two extremes of the tiltrotor UAV functioning modes, rotary-wing and fixed-wing, the control allocation should rely on different actuators. For example, the elevons should mainly be used when the UAV is functioning more similarly to a fixed-wing aircraft. Hybrid approaches handle this problem outright by directly defining separate allocation schemes, considering the different actuators used in each mode. As we wish to consider the system as a whole, depending on the state of the UAV at each instant, the control allocation strategy should be able to calculate the necessary input values without *a priori* information of the functioning modes.

The trajectories considered in this dissertation, which will be described in Chapter 6, deal mostly with longitudinal motion and, as such, in this control allocation scheme, longitudinal motion will be given more significance than lateral motion. Longitudinal motion is linked to the forces in the $\hat{\boldsymbol{\imath}}_{\mathcal{B}}$ and $\hat{\boldsymbol{k}}_{\mathcal{B}}$ directions, $F_{\text{ref,i}}$ and $F_{\text{ref,k}}$, as well as the moment in the $\hat{\boldsymbol{\jmath}}_{\mathcal{B}}$ direction, i.e. the pitching moment $M_{\text{ref,j}}$. These forces and moment, defined in Chapter 4, depend on the rotors' angular velocities ω_1, ω_2, ω_{tr}, the tilt

angles of the front rotors γ_1, γ_2, and the combined elevon angles, which make the elevator angle δ_e. The dependence on these inputs is nonlinear, which complicates the allocation problem. As we want the forces and moment generated by the actuators to follow the references, the following optimisation problem is formulated:

$$\begin{aligned}
&\underset{\omega_1,\,\omega_2,\,\omega_\mathrm{tr},\,\gamma_1,\,\gamma_2,\,\delta_\mathrm{e}}{\text{minimise}} && \left\| \begin{bmatrix} F_{\mathrm{ref,i}} \\ F_{\mathrm{ref,k}} \\ M_{\mathrm{ref,j}} \end{bmatrix} - \begin{bmatrix} F_{\mathrm{input,i}}(\omega_1,\,\omega_2,\,\omega_\mathrm{tr},\,\gamma_1,\,\gamma_2,\,\delta_\mathrm{e}) \\ F_{\mathrm{input,k}}(\omega_1,\,\omega_2,\,\omega_\mathrm{tr},\,\gamma_1,\,\gamma_2,\,\delta_\mathrm{e}) \\ M_{\mathrm{input,j}}(\omega_1,\,\omega_2,\,\omega_\mathrm{tr},\,\gamma_1,\,\gamma_2,\,\delta_\mathrm{e}) \end{bmatrix} \right\|_2 , \\
&\text{subject to} && 0 \leq \omega_1 \leq \omega_{1,\max} \\
& && 0 \leq \omega_2 \leq \omega_{2,\max} \\
& && 0 \leq \omega_\mathrm{tr} \leq \omega_{\mathrm{tr},\max} \\
& && 0 \leq \gamma_1 \leq \gamma_{1,\max} \\
& && 0 \leq \gamma_2 \leq \gamma_{2,\max} \\
& && \delta_{\mathrm{e},\min} \leq \delta_\mathrm{e} \leq \delta_{\mathrm{e},\max}
\end{aligned} \tag{5.23}$$

which is solved at each time instant by a nonlinear optimisation solver. Taking the aforementioned inputs as variables and attempting to minimise the difference between the reference forces and moment and those generated by the actuators should give the necessary input values.

Regarding lateral motion, the lateral aerodynamic force and moments, in terms of inputs, depend linearly on the aileron angle δ_a, the difference between the left and right elevon angles, as is shown in (4.12)-(4.14). In terms of the rotors, lateral motion can be achieved via differential thrust, depending on their direction, given by the tilt angle. Considering the trajectories and to simplify the problem of computing the differential thrust of the front rotors, an equal tilt angle γ is assumed, given by the average of the angles calculated in (5.23), making the lateral moments related to the rotors dependent on $\omega_\mathrm{d} = (\omega_1^2 - \omega_2^2)$. Taking δ_a and ω_d as the variables, the allocation problem for the lateral motion is formulated as the following constrained least squares problem

$$\begin{aligned}
&\underset{\omega_\mathrm{d},\delta_\mathrm{a}}{\text{minimise}} && \left\| \begin{bmatrix} 0 & 0.5\,\rho\,S\,(1-\sigma(\alpha))\,C_{\mathrm{Y_a}} \\ -r_{1,\mathrm{y}}\,k_\mathrm{F}\,\sin(\gamma) & 0.5\,\rho\,S\,b\,(1-\sigma(\alpha))\,C_{\mathrm{l_a}} \\ -r_{1,\mathrm{y}}\,k_\mathrm{F}\,\cos(\gamma) & 0.5\,\rho\,S\,b\,(1-\sigma(\alpha))\,C_{\mathrm{n_a}} \end{bmatrix} \begin{bmatrix} \omega_\mathrm{d} \\ \delta_\mathrm{a} \end{bmatrix} - \begin{bmatrix} F_{\mathrm{ref,j}} \\ M_{\mathrm{ref,i}} \\ M_{\mathrm{ref,k}} \end{bmatrix} \right\|_2^2 , \\
&\text{subject to} && \delta_{\mathrm{a},\min} \leq \delta_\mathrm{a} \leq \delta_{\mathrm{a},\max}
\end{aligned} \tag{5.24}$$

which is solved at each time instant, after problem (5.23). Denoting by $\omega_\mathrm{c} = (\omega_1^2 + \omega_2^2)$ the sum of the squared front rotors' spin velocity obtained from (5.23), and having computed ω_d, δ_e and δ_a, the final front rotors' spin velocities ω_1 and ω_2, and the right and left elevon angles, $\delta_{\mathrm{e,r}}$ and $\delta_{\mathrm{e,l}}$, are obtained by

$$\begin{aligned}
\omega_1 &= \sqrt{\frac{\omega_\mathrm{c}}{2} + \frac{\omega_\mathrm{d}}{2}}\,, & \delta_{\mathrm{e,r}} &= \frac{\delta_\mathrm{e}}{2} - \frac{\delta_\mathrm{a}}{2}\,, \\
\omega_2 &= \sqrt{\frac{\omega_\mathrm{c}}{2} - \frac{\omega_\mathrm{d}}{2}}\,, & \delta_{\mathrm{e,l}} &= \frac{\delta_\mathrm{e}}{2} + \frac{\delta_\mathrm{a}}{2}\,.
\end{aligned} \tag{5.25}$$

This control allocation approach presents some limitations that will be addressed in the following section.

5.4 Limitations

The control and allocation strategies described throughout this chapter have some limitations that will now be discussed.

First, the backstepping approach depends on the assumed aerodynamic model, hence requiring a good knowledge of the coefficients and parameters described in Chapter 4. It is then necessary to study the aerodynamics of the aircraft with, for example, wind tunnel tests or computational fluid dynamics simulations.

Another issue concerns the calculation of the attitude reference. As was mentioned, the UAV's pitch angle influences the calculation of γ_{est}, which is addressed by assuming that the aircraft's pitch angle is always constrained between $\theta_{\min}$ and $\theta_{\max}$. Despite this being adequate for the normal functioning of tiltrotor aircraft, it might not hold at all times and could then jeopardise the computation of the orientation reference in (5.11). Moreover, formulating the orientation reference generation as a nonlinear optimisation problem creates further issues. The solver may take more time than acceptable to solve the problem, leaving the aircraft without a correct orientation reference. This problem may be minimised by, for example, using the solution of a certain time instant as the initial guess of the following instant. For the trajectories considered, the orientation reference should not change substantially from one time instant to the next, so the solver should take less iterations to compute the current reference. The results may also vary depending on the nonlinear optimisation solver used.

The control allocation strategy poses a similar problem, as the solver may not be able to compute the solution in the necessary time interval. As before, using a certain solution as the initial guess of the following time instant could reduce the computation time, though, in the case of the inputs, the solutions will vary more significantly throughout the trajectory, when compared to the changes in the orientation reference. Nevertheless, an optimisation approach is not ideal and further work is required to make this controller reliable and viable in a real world application. A closed-form solution to this problem would be preferable, as was the one presented in [21], discussed in Chapter 2, in which the system dynamics are linearised around a predefined trim point and a pseudo-inverse of the input effectiveness matrix computed. However, such a solution to the allocation problem is difficult to obtain without a trade-off, as in the case mentioned the tilt angles were limited and the UAV could not fly in a fully fixed-wing mode. Moreover, the division of the allocation problem into longitudinal and lateral dynamics, instead of considering everything at once, was made to reduce the complexity of the optimisation problem. It gives more significance to the longitudinal dynamics, which play a larger role in the trajectories considered, at the expense of the lateral dynamics, but a solution that takes into account the longitudinal and lateral

dynamics simultaneously would be preferable, so as not to compromise the necessary lateral force and moment allocation.

6

Simulation Results

Contents

In this chapter, the simulation results are presented for two trajectories that are introduced next. The tiltrotor UAV is set to initially be at rest, at the origin of the inertial frame, and with its body frame aligned with the inertial frame. The effect of wind is not considered in the simulations. As the values of the *E-flite Convergence VTOL* UAV model parameters and coefficients are not known, the values used in simulation are adapted from those presented in [28] for the fixed-wing UAV Aerosonde. The model and simulation parameters are presented in Appendix A. The simulations were performed using Matlab and Simulink.

6.1 Reference Trajectories

The intended behaviour is to have the UAV take off, fly in hover mode up until a certain altitude and from there transition into a forward level flight. The choice of trajectory combines the concepts of trim trajectories and trapezoidal velocity profile trajectories used in [12, 16]. A trim trajectory is characterised by the total forces and moments acting on the aircraft summing to zero, i.e. both the linear and angular accelerations, with respect to the aircraft, are null. This implies that linear velocity, the pitch and roll angles, as well as the yaw rate, are constant. Level flight and circular curves are usual examples of trim trajectories.

The trajectories will be divided into two segments, upwards and forwards, to simplify the analysis. Two trajectories are calculated: in the first, the UAV is expected to fully transition into a trim level flight, and in the second, it transitions into a forward trajectory with a velocity lower than trim.

6.1.1 Upward Trajectory Segment

The UAV starts at an initial position $\mathbf{p}_0$, which can be defined without loss of generality as $\mathbf{p}_0 = \begin{bmatrix} 0 & 0 & 0 \end{bmatrix}^\mathsf{T}$ m. Starting at rest, the intention is to fly in the negative $\hat{\boldsymbol{k}}_\mathcal{I}$-direction until it reaches a certain altitude h, with $h > 0$, thus being at position $\mathbf{p}_\mathrm{h} = \begin{bmatrix} 0 & 0 & -h \end{bmatrix}^\mathsf{T}$.

To have an upwards trim trajectory, the UAV's acceleration must be null, i.e. the sum of the forces acting on the UAV must also be null. Discarding the aerodynamic forces in this segment of the trajectory due to their small magnitude, it follows that the thrust generated by the rotors must cancel the force of gravity. However, since the aircraft starts at rest, this would mean that it would hover continuously at $\mathbf{p}_0$. Therefore, the UAV must first be accelerated upwards to gain velocity. Afterwards, if the overall acceleration is zero, the UAV will still move upwards, due to its momentum, at the velocity it achieved. To then stop at a certain point, it should decelerate by generating less thrust. If the acceleration at the beginning and at the end are constant values, the resulting trajectory is defined as a trapezoidal velocity profile trajectory.

As such, for the upward trajectory segment, starting at rest from position $\mathbf{p}_0$, first the aircraft accelerates upwards at $\mathbf{a}_1 = \begin{bmatrix} 0 & 0 & a_1 \end{bmatrix}$, with $a_1 < 0$, until it achieves an upwards velocity $\mathbf{v}_{\text{up}} = \begin{bmatrix} 0 & 0 & v_{\text{up}} \end{bmatrix}$, with $v_{\text{up}} < 0$. Then, the velocity is kept constant, meaning the acceleration is null. After a certain amount of time, the UAV starts decelerating so as to hover at $\mathbf{p}_{\text{h}}$. That amount of time depends on the choice of the acceleration $\mathbf{a}_2 = \begin{bmatrix} 0 & 0 & a_2 \end{bmatrix}$, with $a_2 > 0$ at which the UAV decelerates, in order to complete the trapezoidal velocity profile. Note that since only upward motion is intended, the desired velocity and acceleration in the $\hat{\boldsymbol{\imath}}_{\mathcal{I}}$ and $\hat{\boldsymbol{\jmath}}_{\mathcal{I}}$-directions is zero at all times.

6.1.2 Forward Trajectory Segment

Regarding the forward trajectory segment, the objective is to go from hover at position $\mathbf{p}_{\text{h}}$ to a forward level flight at the same altitude. To accomplish this, the UAV needs to accelerate forward. To simplify, and without loss of generality, it was chosen that the acceleration would be in the (positive) direction of the $\hat{\boldsymbol{\imath}}_{\mathcal{I}}$-axis. As such, the UAV first accelerates at $\mathbf{a}_{\text{for}} = \begin{bmatrix} a_{\text{for}} & 0 & 0 \end{bmatrix}$, until it reaches the desired forward velocity $\mathbf{v}_{\text{for}} = \begin{bmatrix} v_{\text{for}} & 0 & 0 \end{bmatrix}$, which is kept constant from then on.

In forward flight, the aerodynamic effects cannot be ignored as before. In the case of trim level flight, the force of gravity, the aerodynamic forces, and the rotor forces sum to zero, and the aircraft's velocity is constant and needs to be calculated. Since the aerodynamic forces depend on the velocity and angle of attack of the aircraft in a nonlinear fashion, calculating the trim conditions is more challenging. Certain assumptions or requirements can be made in order to simplify the problem. Since in level flight the UAV is supposed to behave like a fixed-wing aircraft, it is logical to assume that both front rotors will be completely tilted forward and that the tail rotor is motionless. In addition, one may further assume a certain angle of attack. Different angle of attack values will produce different trim velocity norm values.

As in this trajectory segment the motion should be exclusively forward (the aircraft should not lose altitude) and in the $\hat{\boldsymbol{\imath}}_{\mathcal{I}}$-direction, the desired velocity and acceleration in the $\hat{\boldsymbol{\jmath}}_{\mathcal{I}}$ and $\hat{\boldsymbol{k}}_{\mathcal{I}}$-directions is zero. Note that this trajectory segment is not truly a trapezoidal velocity profile trajectory since, after achieving constant velocity level flight, the reference is kept in this condition. As such, the aircraft does not decelerate back to rest in hover, since the UAV has to rely on drag to decelerate instead of its actuators, which makes this manoeuvre more complex. Hence, this manoeuvre requires further research to be performed and is not addressed in this dissertation.

6.1.3 Complete Reference Trajectory

The complete reference trajectory is simply the concatenation of the two aforementioned segments. Figures 6.1, 6.2, and 6.3 show the position, velocity, and acceleration profiles, respectively, in the $\hat{\boldsymbol{\imath}}_{\mathcal{I}}$, $\hat{\boldsymbol{\jmath}}_{\mathcal{I}}$, and $\hat{\boldsymbol{k}}_{\mathcal{I}}$ axes, of two trajectories denoted by Trajectory A and Trajectory B. In Trajectory A, the forward

velocity is the trim velocity of the simulated aircraft model, whereas in Trajectory B, the forward velocity is approximately 10 m/s less than trim, which corresponds to ≈ 70% of the trim velocity. Both trajectories will be used as references in the simulations presented next.

Trajectory A and B share the same upwards trajectory segment. The final position is defined as $\mathbf{p}_{\mathrm{h}} = \begin{bmatrix} 0 & 0 & -2 \end{bmatrix}$ m, i.e at an altitude of 2 m. The acceleration values are $a_1 = -0.1$ m/s^2 and $a_2 = 0.1$ m/s^2, and the constant velocity value is $v_{\mathrm{up}} = -0.2$ m/s.

Regarding the forward segment, the acceleration value is $a_{\mathrm{for}} = 7.5$ m/s^2 for both trajectories. As aforementioned, the difference lies in the forward velocity values, which is the trim velocity $v_{\mathrm{for}} = 35.75$ m/s, for Trajectory A, and a lower value of $v_{\mathrm{for}} = 25$ m/s, for Trajectory B. The trim velocity value was calculated assuming an angle of attack of zero degrees. The reference acceleration values were tuned in simulation.

The upward segment takes place in the time interval $t = [0,\ 12]$ s, followed by the forward segment from then on. The plots are truncated at $t = 24$ s. As may be seen in Figure 6.3, both the accelerating and decelerating parts of the upwards segment have a duration of two seconds. The accelerating part of the forward trajectory segment lasts approximately 4.7 s, in Trajectory A, and approximately 3.33 s, in Trajectory B.

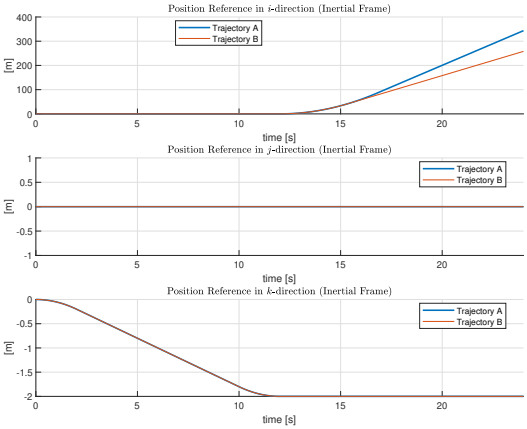

Figure 6.1: Position Reference

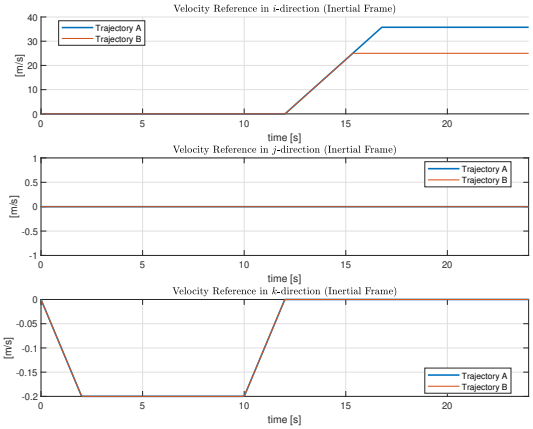

Figure 6.2: Velocity Reference

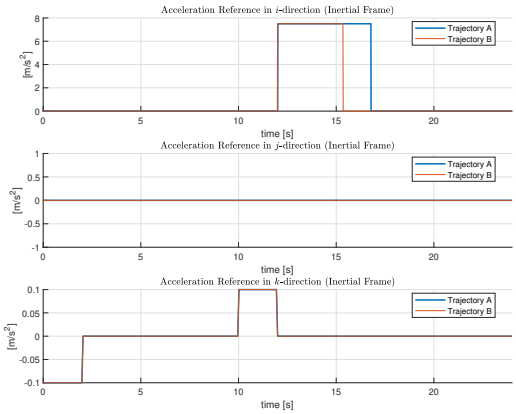

Figure 6.3: Acceleration Reference

6.2 Trajectory with Forward Trim Velocity

This section concerns the simulation results obtained with the trajectory previously designated by Trajectory A, in which the tiltrotor UAV is supposed to fly forward at trim velocity.

Figures 6.4 and 6.5 show the plots of the reference and actual position and velocity, respectively. The UAV is able to follow the reference trajectory, climbing to an altitude of $2\,\text{m}$ in the first $12\,\text{s}$ and moving forward from then on at the same altitude. The aircraft also adequately tracks the velocity reference, especially in the $\hat{\boldsymbol{\imath}}_{\mathcal{I}}$ and $\hat{\boldsymbol{\jmath}}_{\mathcal{I}}$ axes, keeping its velocity at zero in both directions during the upward segment, following the forward velocity reference during the acceleration part of the forward flight segment, and stabilising at the trim velocity. Regarding the velocity reference tracking in the $\hat{\boldsymbol{k}}_{\mathcal{I}}$ axis, one notices that during the upward motion, the aircraft tracks the reference, but there is a small error when it begins moving forward. In fact, when the transition, i.e the forward acceleration part of the trajectory, begins at $t = 12\,\text{s}$ and when the tail rotor reduces its angular velocity at $t = 15.5\,\text{s}$, the UAV gains downward velocity, but is able to correct it and stay levelled. In general, the aircraft is able to track the position reference, as well as the velocity, when transitioning from hover into forward flight.

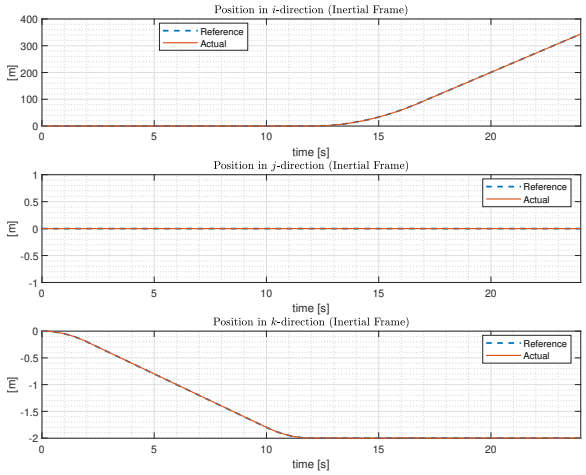

Figure 6.4: Trajectory A: Position

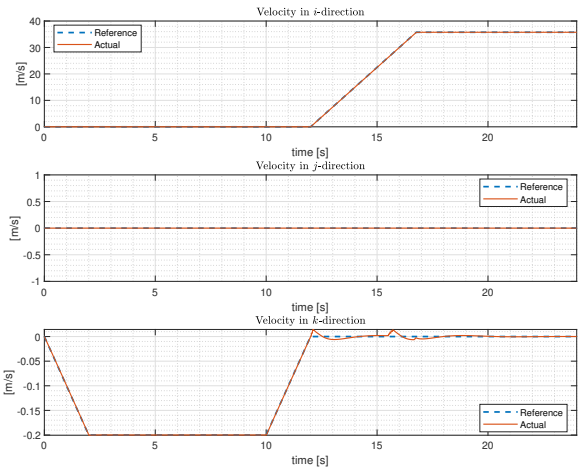

Figure 6.5: Trajectory A: Velocity

The results regarding the orientation and angular velocity are presented in Figures 6.6 and 6.7. The orientation results are described in Euler angles for a more intuitive analysis. One concludes that the attitude reference generated by the position controller only acts on the longitudinal dynamics, which is reasonable since only forward motion is required. It is also noticeable that the aircraft is not always able to follow the orientation and angular velocity references, particularly at the beginning and end of the forward acceleration part of the trajectory, similar to the tracking of the vertical linear velocity. At these points, the orientation reference presents some brief spikes to negative pitch values on an otherwise constant reference of zero pitch angle, with the largest spike in terms of magnitude having a value of, approximately, $-0.12\,\text{rad}$. Despite the reference spikes, the pitch angle remains close to zero throughout

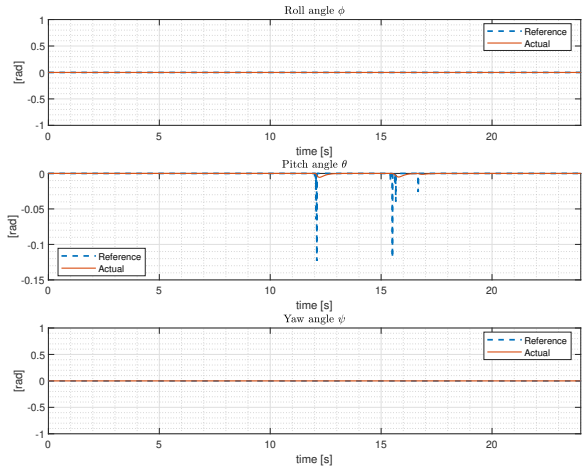

Figure 6.6: Trajectory A: Orientation

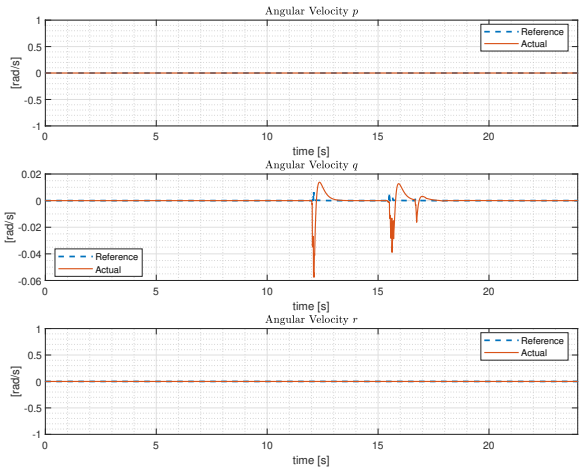

Figure 6.7: Trajectory A: Angular velocity

the trajectory, deviating at most to a pitch of -0.005 rad, approximately. The pitching angular velocity q follows the reference after the spikes that result from the beginning and end of the forward acceleration, despite presenting overshoot.

The forces and moments allocated by the control allocation scheme and generated by the actuators, with respect to the body frame, are shown in Figures 6.8 and 6.9. Considering first the force, during the upwards segment, the reference in the $\hat{\boldsymbol{\imath}}_{\mathcal{B}}$ and $\hat{\boldsymbol{\jmath}}_{\mathcal{B}}$ axes is zero, and in the $\hat{\boldsymbol{k}}_{\mathcal{B}}$ axis opposes the force of gravity, with a value of -132.4 N, and with a slightly larger magnitude during the upward acceleration and slightly smaller during the deceleration, as would be expected. As the aircraft starts moving forward, there is a sharp increase in the forward force reference as soon as it begins accelerating. The reference force keeps increasing up until the point when the aircraft stops accelerating, then stabilising at approximately 39.8 N. On the other hand, the reference in the $\hat{\boldsymbol{k}}_{\mathcal{B}}$ axis decreases in magnitude as the UAV moves forward, since more lift force is being generated by the wings, and less is required of the rotors to counteract the effect of gravity. At trim velocity the vertical force reference is approximately -7.5 N. The force reference in the $\hat{\boldsymbol{\jmath}}_{\mathcal{B}}$ axis is zero throughout the trajectory. Examining the moments, it is clear that during the upward motion, the required moments in all body axes are zero, since the aircraft's attitude should remain constant during this part of the trajectory. Since the attitude only changes in terms of the pitch angle, it is natural that the moment reference only changes in the $\hat{\boldsymbol{\jmath}}_{\mathcal{B}}$ axis and remains zero in the other two, as observed. In trim flight, the pitching moment reference stabilises at, approximately, 2 Nm, and during the accelerating phase it presents two brief spikes of approximately -5 Nm, the first caused by the beginning of the forward acceleration and the second coinciding with the severe reduction of the tail rotor angular velocity at $t = 15.5$ s, which has implications on the pitching moment, and a third spike of approximately 0.42 Nm at the time that the aircraft stops accelerating. In spite of these short spikes, overall, the pitching moment reference increases from 0 Nm at hover to 2 Nm at trim level flight. From

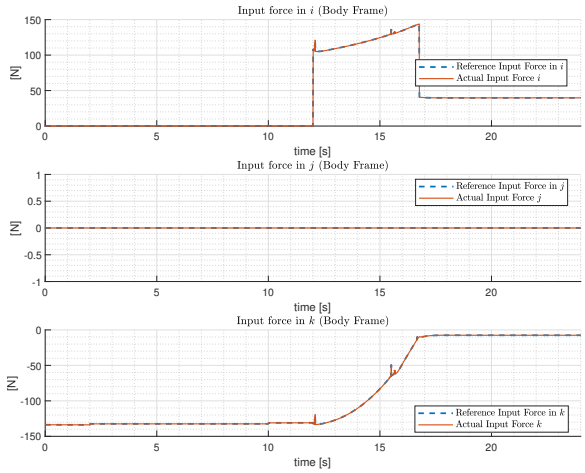

Figure 6.8: Trajectory A: Force in body

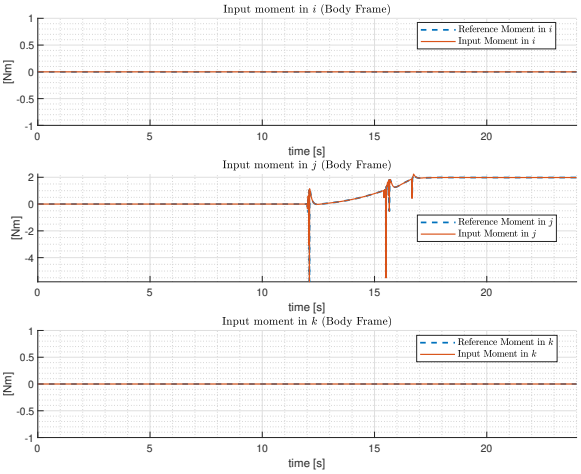

Figure 6.9: Trajectory A: Moment in Body

the plots, one concludes that the control allocation scheme is able to follow and allocate the reference force and moment through the trajectory.

Figures 6.10 and 6.11 show the input values, i.e. rotors' angular velocities as well as the tilt and elevon angles, throughout the trajectory. During the upward segment, the rotors speed stays almost constant, with the front rotors spinning at approximately 6.9 rad/s and the tail rotor at 5.0 rad/s, though with slightly more speed in the accelerating part and less in the decelerating part. The tilt rotors point upwards and the elevon angles are kept at zero throughout this part of the trajectory, as they do not play a significant role. For the second part of the trajectory, the front rotors increase their angular velocity and tilt forward at approximately $43°$ to begin accelerating forward, and the elevons deflect upwards at approximately -0.5 rad to compensate the pitching motion. As the UAV accelerates forward, the front rotors' angular velocities keeps increasing and the tail rotor's angular velocity decreases. When the aircraft reaches trim velocity, the front rotors' angular velocities decreases moderately and stabilises at 13.6 rad/s, and the tail rotor stops. During the accelerating part, the tilt angles initially decrease to a value of approximately $14°$, but increase again to $33°$ at $t = 15.7$ s, which compensates the loss of lift that results from the tail rotor's angular velocity diminishing. From then on, the tilt angles decrease once again and stabilise at zero during trim forward flight. Regarding the elevons, after initially deflecting upwards, they begin to deflect downwards and stay at approximately -0.02 rad in trim forward flight.

On the whole, the UAV is able to follow the defined trajectory, keeping a levelled attitude throughout, and the required forces and moments are allocated. Furthermore, by analysing the plots, it becomes clear that, at forward trim velocity, the tail rotor stops spinning and the front rotors are fully tilted forwards, meaning that the UAV is functioning as a fixed-wing aircraft, as supposed.

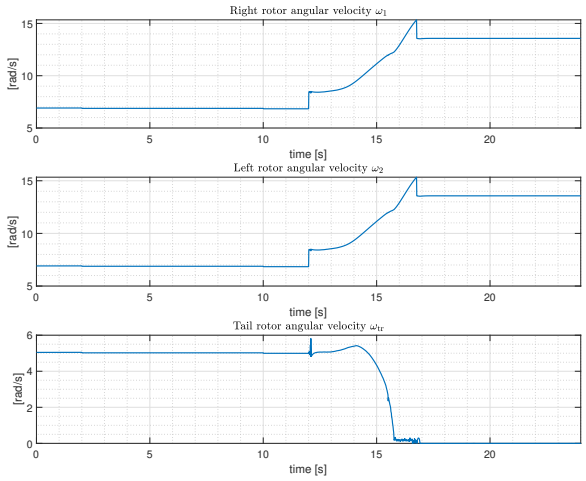

Figure 6.10: Trajectory A: Rotors' angular velocities

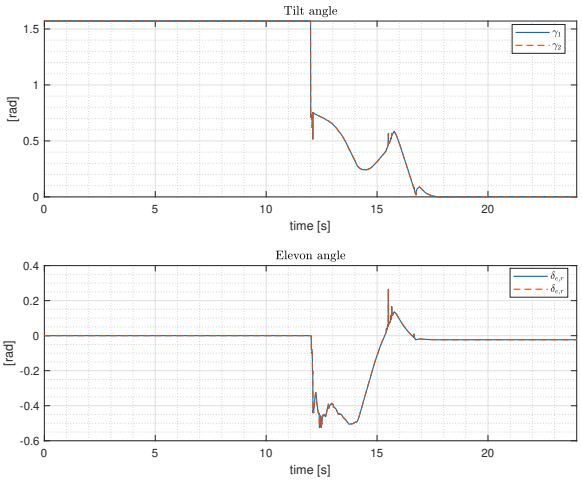

Figure 6.11: Trajectory A: Tilt and Elevon angles

6.3 Trajectory with Forward Sub-trim Velocity

In this section, the simulation results obtained with the trajectory previously designated by Trajectory B, in which the tiltrotor UAV is supposed to fly forward at a velocity lower than trim, are analysed.

Considering first the following of the position and velocity references, show in Figures 6.12 and 6.13, respectively, one notices that the results are similar to those obtained for the previous trajectory. The position is followed, with the UAV climbing to an altitude of $2\,$m in the first $12\,$s, without moving in the $\hat{\boldsymbol{\imath}}_{\mathcal{I}}$ and $\hat{\boldsymbol{\jmath}}_{\mathcal{I}}$ axes, and keeping that altitude while moving forward in the $\hat{\boldsymbol{\imath}}_{\mathcal{I}}$ direction from then on. The actual velocity follows the reference, with only minor errors in the $\hat{\boldsymbol{k}}_{\mathcal{I}}$ axis reference. In the other two axes, the velocity is kept at zero during the upward segment of the trajectory and increases in the $\hat{\boldsymbol{\imath}}_{\mathcal{I}}$ axis during the acceleration part until stabilising at $25\,$m/s, at $t = 15.3\,$s. The vertical velocity decreases initially in the $\hat{\boldsymbol{k}}_{\mathcal{I}}$ axis as the aircraft begins climbing upwards, reaching a velocity of $-0.2\,$m/s before decelerating to remain at the desired altitude. As it starts accelerating in the $\hat{\boldsymbol{\imath}}_{\mathcal{I}}$ direction, the vertical velocity increases momentarily before once again stabilising at zero.

Figures 6.14 and 6.15 show, respectively, the orientation and angular velocity results. At first, during the upward trajectory segment, everything is akin to the previous case, as the upward segment in both cases is the same. The orientation reference is such that it keeps the UAV levelled, with roll and pitch angles of zero, and the angular velocity reference is also zero for all axes, and the aircraft follows these references as expected. The roll and yaw angles are zero for the entirety of the trajectory, as only longitudinal motion is required. Then, as the forward trajectory segment begins at $t = 12\,$s, one observes the first major dissimilarities. As soon as the UAV starts accelerating forward, the pitch angle reference presents a brief spike of approximately $-0.12\,$rad, which the vehicle does not follow, though a small decrease in pitch angle can be observed, and it then goes zero and stays at this value until $t = 15.3\,$s, when the UAV stops accelerating. The angular velocity during this period is as expected, with a spike

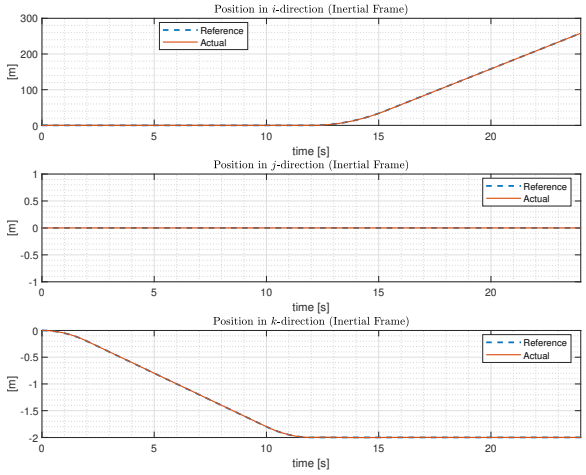

Figure 6.12: Trajectory B: Position

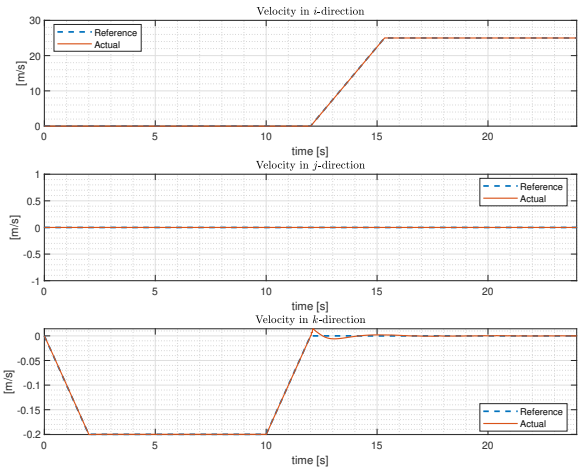

Figure 6.13: Trajectory B: Velocity

to a negative value at first, approximately -0.058 rad/s, compensating afterwards with some overshoot to then stabilise at zero. After $t = 15.3$ s, as the UAV is flying at 25 m/s, the behaviour becomes more irregular, as can be seen in Figures 6.16 and 6.17, with the pitch angle reference presenting several brief spikes, with zero value in between, contributing to small oscillations of the actual value of the pitch angle. The angular velocity also presents irregular behaviour, though of small magnitude, despite an almost constant reference of zero, with some short spikes. As this trajectory no longer qualifies as trim, the total forces and moments acting on the aircraft is not zero, which contributes to this erratic behaviour, different to the one observed in the previous case.

Let us now analyse the forces and moments generated by the actuators, shown in Figures 6.18 and 6.19, respectively. During the upward segment, the forces and moments are equal to those described in the previous section. As soon as the aircraft starts accelerating forward, there are brief spikes in the forces in the $\hat{\boldsymbol{\imath}}_{\mathcal{B}}$ and $\hat{\boldsymbol{k}}_{\mathcal{B}}$ axes and in the moment in the $\hat{\boldsymbol{\jmath}}_{\mathcal{B}}$ axis. The force in $\hat{\boldsymbol{\imath}}_{\mathcal{B}}$ keeps increasing during the forward acceleration part of the trajectory, reaching a maximum of 127.2 N, and the force in $\hat{\boldsymbol{k}}_{\mathcal{B}}$ decreases, in terms of magnitude, to -70.4 N, as more lift force is generated by the wings, which counteracts the force of gravity. The moment in $\hat{\boldsymbol{\jmath}}_{\mathcal{B}}$ also increases to approximately 1.2 Nm. It is interesting to note that since the tail rotor does not stop, as will be seen, there are no irregularities in the forces and moments due to this, as there were in the case of the previous trajectory in the forwards acceleration part at $t = 15.5$ s. Once again, at $t = 15.3$ s, the behaviour changes, with the force in $\hat{\boldsymbol{\imath}}_{\mathcal{B}}$ decreasing abruptly to an approximate value of 23.3 N, with some oscillations, and the force in $\hat{\boldsymbol{k}}_{\mathcal{B}}$ staying at approximately -72.2 N, also displaying erratic behaviour. The pitching moment also exhibits irregular behaviour akin to the forces and the pitch angle and angular velocity element q. Despite the irregularities, the allocated forces and moments follow the respective references. The force in $\hat{\boldsymbol{\jmath}}_{\mathcal{B}}$, as well as the moments in $\hat{\boldsymbol{\imath}}_{\mathcal{B}}$ and $\hat{\boldsymbol{k}}_{\mathcal{B}}$, are zero throughout the trajectory, similar to the results obtained with the previous trajectory.

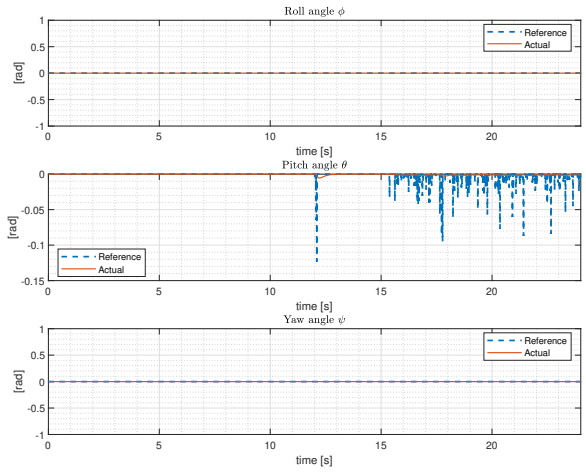

Figure 6.14: Trajectory B: Orientation

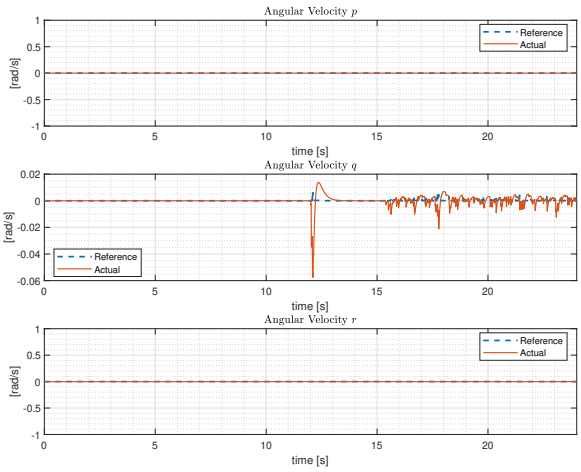

Figure 6.15: Trajectory B: Angular velocity

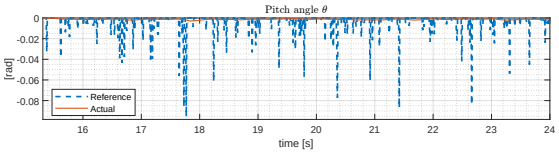

Figure 6.16: Trajectory B: Pitch angle θ during forward flight $t = [15.3,\ 24]$ s (detailed)

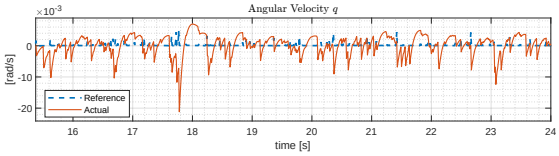

Figure 6.17: Trajectory B: Angular velocity q during forward flight $t = [15.3,\ 24]$ s (detailed)

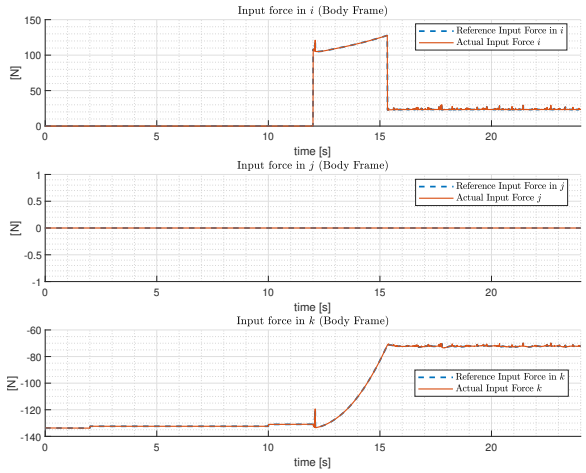

Figure 6.18: Trajectory B: Force in body

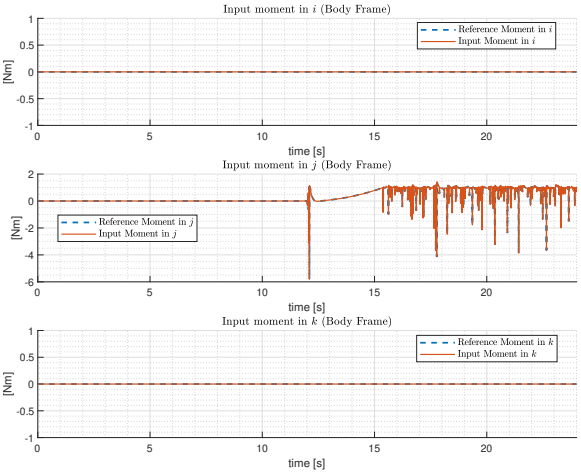

Figure 6.19: Trajectory B: Moment in Body

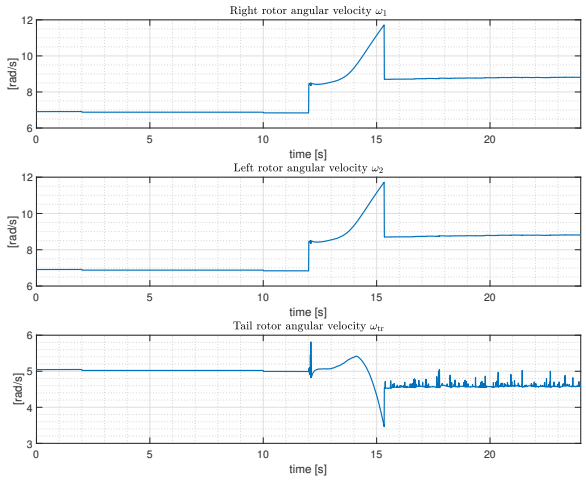

Figure 6.20: Trajectory B: Rotors' angular velocities

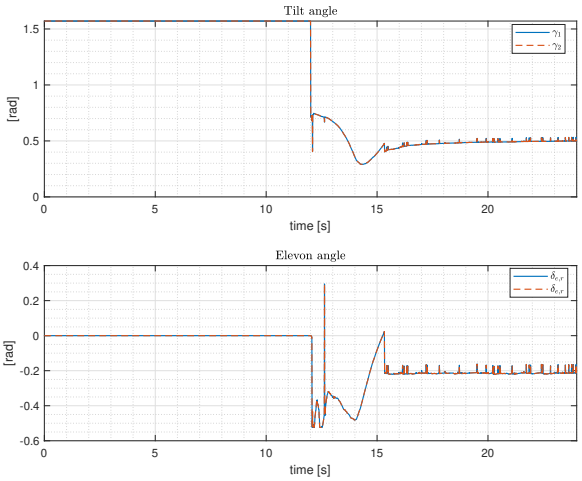

Figure 6.21: Trajectory B: Tilt and Elevon angles

Considering the rotors' angular velocities as well as the tilt and elevon angles, throughout the trajectory, presented in Figures 6.20 and 6.21, once more the behaviour during first segment of the trajectory is equal to the previous case. Analysing the inputs as the aircraft stops accelerating forward, at $t = 15.3$ s, one notices a sharp reduction in the angular velocities of the front rotors to a value of approximately 8.7 rad/s and a sharp increase in the tail rotor's angular velocity to approximately 4.6 rad/s. The tail rotor's angular velocity also presents irregular behaviour, unlike the previous case where it stabilised at zero, which contributes to the irregular pitching moment, since it is directly influenced by this rotor. The tilt angles, which start off at approximately $43°$ and initially decrease to $17.1°$, eventually stabilise at $28.6°$, despite some brief small magnitude spikes, during forward flight at 25 m/s. The elevon deflection angles present a behaviour similar to that of the previous trajectory, initially deflecting upwards, then deflecting downwards as the UAV gains velocity, this time stabilising at -0.21 rad, and also displaying brief small magnitude spikes.

Taking everything into account, one concludes that the UAV's behaviour along this trajectory is not as smooth as it is along a trim trajectory, which is understandable. Nevertheless, the vehicle is able to fly in an intermediate state in forward flight, not in fully rotary-wing nor fixed-wing mode, with the front rotors tilted at a certain angle, in this case, at $28.6°$, and with its tail rotor still rotating, which was the objective.

7

UAV Instrumentation

Contents

This chapter describes the instrumentation of the *E-Flite Convergence VTOL* with an autopilot compatible with PX4 flight control software. To validate the instrumentation, a flight in an arena equipped with a motion capture system was carried out.

7.1 Instrumentation

The objective is to equip an *E-Flite Convergence VTOL* with a PX4-compatible autopilot that will allow to control the UAV via remote control and with a ground station, to perform real flight tests, as well as to implement and test different control algorithms. Due to the size of the vehicle and the space available, the chosen autopilot is a Pixhawk 4 Mini, by Holybro and Auterion, shown in Figure 7.1. The autopilot comes with a GPS module that provides global position and compass data, Figure 7.2, and a power module that supplies regulated power to the flight controller, Figure 7.3.

The Pixhawk 4 Mini weighs only 37.2 g and its dimensions are 38×55×15.5 mm, making it appropriate for small UAVs. It has a Flight Management Unit with a 32-bit Arm Cortex-M7, 216 MHz, 2 MB memory, 512 KB RAM, and is equipped with two accelerometers and gyroscopes, a magnetometer and a barometer. It also includes eight Pulse-Width Modulation (PWM) output ports (MAIN ports), of which seven will be used, four PWM/Capture input ports, a dedicated port for the GPS module, a Radio Control (RC) input port (RC IN), a telemetry port (TELEM1), a CAN bus port, a UART and I2C compatible port, and finally a power port that connects to the power module [31].

Communication with the autopilot is done via radio and WiFi. As such, the vehicle is equipped with a FrSky RX8R radio receiver which connects to the RC IN port of the Pixhawk 4 Mini, Figure 7.4, to fly the UAV in RC mode, and with an ESP8266 WiFi module which connects to the TELEM1 port, Figure 7.5, to communicate via WiFi with a ground control station.

The *E-Flite Convergence VTOL* has three rotors with brushless motors, which are controlled by PWM signals. To achieve this, the right motor connects to MAIN 1 port, the left motor connects to MAIN 2 port, and the tail motor connects to MAIN 3 port. To supply power to these motors, the power connections

Figure 7.1: Pixhawk 4 Mini autopilot

Figure 7.2: GPS module

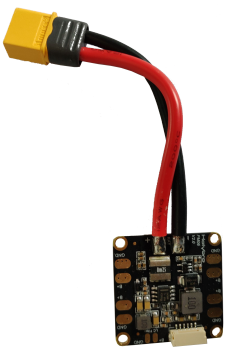

Figure 7.3: Power module

Figure 7.4: FrSky RX8R RC receiver

Figure 7.5: ESP8266 WiFi module

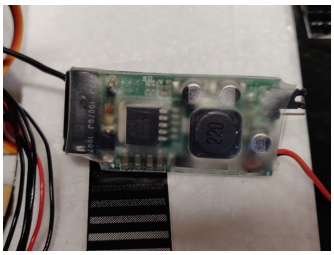

Figure 7.6: Battery Elimination Circuit

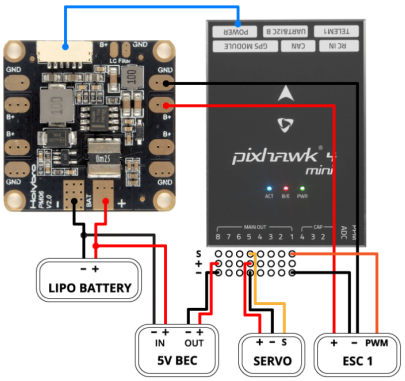

Figure 7.7: Power module connections

are soldered directly to the power module board. The tilt and elevon angles are controlled by servo motors. The right and left tilt servo motors connect to MAIN 5 and 6, respectively, and the right and left elevon servo motors to MAIN 7 and 8, respectively. To connect the servo motors to these ports, a Battery Elimination Circuit (BEC) has to be connected to MAIN 8, which acts as a voltage regulator to power the servo motors. Figure 7.7 shows the connections between the power module and the Pixhawk 4 Mini, with a BEC connected to MAIN 8, a servo motor connected to MAIN 5, and an Electronic Speed Controller (ESC), which converts the PWM signal to drive the brushless motors, connected to MAIN 1. Power is supllied by a 3-cell Li-Po 11.1 V, 2600 mAh battery, which fits on the top of the UAV.

All these components were assembled on the *E-Flite Convergence VTOL*. Figures 7.8(a) and 7.8(b) show the top and bottom view of the UAV, respectively, displaying the arrangement of all the parts. The GPS module was lodged in the front of the UAV, in a compartment especially carved out for it, in front of the battery, which is followed by the WiFi module, placed in a separate compartment. The reflective markers that were mounted on the UAV for usage with the motion capture system are also visible in Figure 7.8(a). The Pixhawk 4 Mini was mounted on the vehicle's bottom compartment, close to the CoM. The power module was placed in a compartment between the autopilot and the tail rotor and the BEC was placed outside the bottom compartment, due to lack of space. The RC receiver was mounted in front of the autopilot.

To eventually implement and test the control approach presented in this dissertation, or another approach different than the one provided by the autopilot, some modifications to the instrumentation will

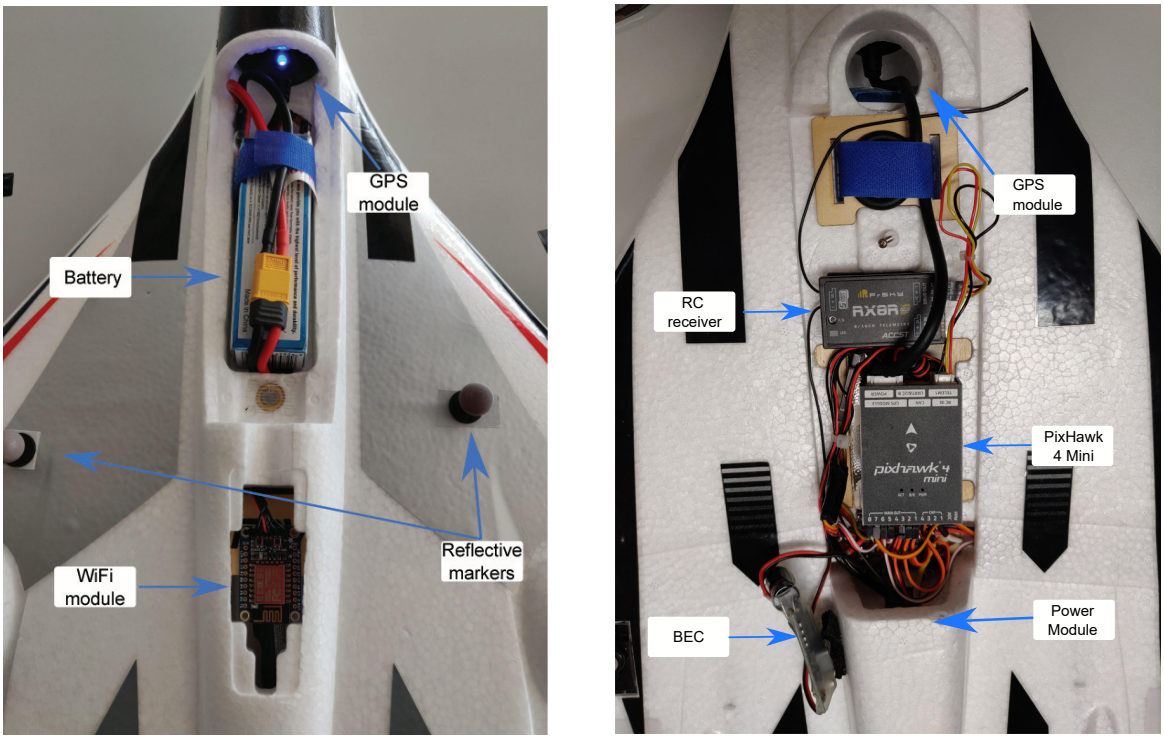

(a) Top view **(b)** Bottom view

Figure 7.8: Assembled components on the *E-flite Convergence VTOL*

be required. In particular, a small computer, designated by companion computer, such as a Raspberry Pi, running Linux and ROS will be mounted on the UAV.

7.2 Validation

To validate the instrumentation, a short test flight was conducted, with the UAV controlled via RC, connected via WiFi to a computer running ground control software. The test was performed in a flight arena equipped with a motion capture system and, therefore, the UAV was flown only in rotary-wing mode. More test flights will be carried out in unconstrained environments to fly the UAV in fixed-wing mode and execute transition manoeuvres. The position data was acquired with the motion capture system, while the velocity, orientation, and angular velocity data were estimated by the autopilot. The results are shown in Figure 7.9. A video of this test flight can be viewed at `https://youtu.be/iLmCVTZQYOs`.

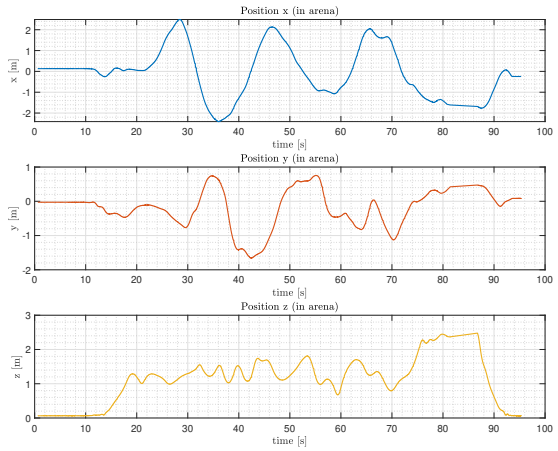

(a) Position

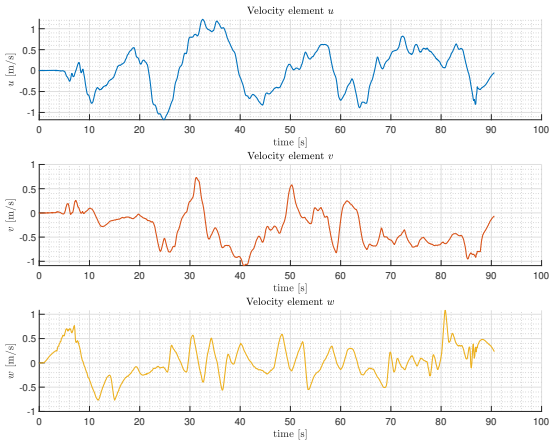

(b) Velocity

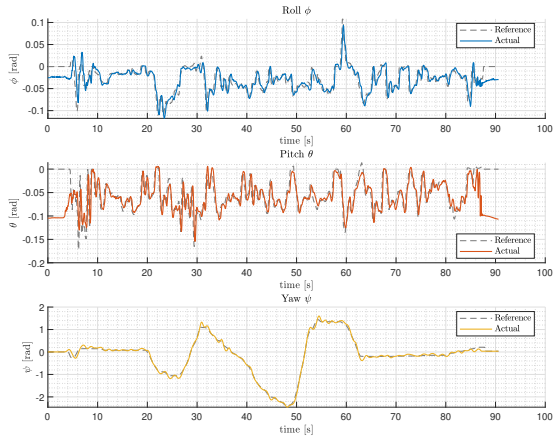

(c) Orientation

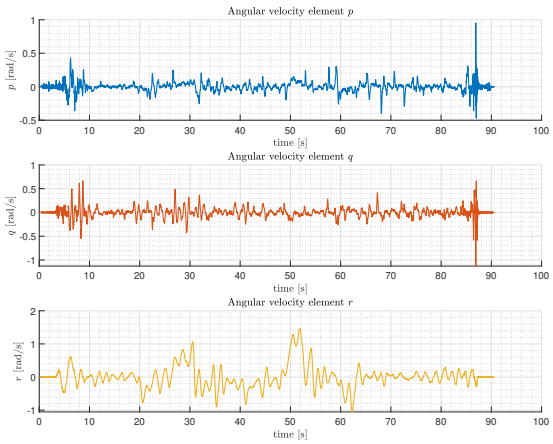

(d) Angular Velocity

Figure 7.9: Validation flight data

8

Conclusion

Contents

In this chapter, we present the conclusions of the work developed throughout this dissertation and discuss the work that remains to be done.

8.1 Conclusions

The main objective of this dissertation was to take the first steps in developing a unified control approach that could be used by hybrid tri-tilrotor UAVs for trajectory tracking.

To meet this goal, first a model of a tri-tilrotor was derived. The inertial and body coordinate frames were defined, along with coordinate frames for each tilting rotor. The forces and moments generated by aerodynamic effects and by the rotors were studied, and the kinematic and dynamic system equations were deduced. To complete the study of the UAV model, the error dynamics were calculated.

Afterwards, the control strategy was devised. The overall control system architecture was presented along with the description of the procedure necessary to have an inner attitude control loop and an outer position control loop, despite the additional difficulty of the degree of freedom that the tilting rotors create. This problem was tackled by assuming an estimate of the rotors' tilt angles and formulating an optimisation problem that gave an orientation reference. Subsequently, the position and attitude controllers were derived. Backstepping control was used for both cases to generate force and moment references, making use of the error dynamics deduced previously, with integral action being added to the position controller. These controllers guaranteed stability, provided that the force and moment references were correctly allocated and followed. Hence, a control allocation scheme was proposed next. The force and moment references related to longitudinal motion were given greater attention, as they would be more relevant in the reference trajectories. These strategies presented some issues and limitations, e.g. the time taken by the optimisation solvers to compute the solution, which were also addressed and discussed.

Then, two trajectories of interest were defined. Each trajectory was composed of an upward motion segment, where the UAV was supposed to fly in a rotary-wing configuration up to a certain altitude, followed by a forward motion segment, in which the UAV should start behaving akin to a fixed-wing aircraft. The two defined trajectories differed in the velocity of the forward motion segment. In the first trajectory, the desired velocity was the trim velocity of the UAV, whereas in the second trajectory, the desired velocity was lower. The purpose of this difference was to observe if in the former the UAV would fully transition into a fixed-wing configuration, with both front rotors tilted forward and the tail rotor stopped, and if in the latter it would fly in an intermediate configuration, with the front rotors tilted somewhere between 0° and 90° and with the tail rotor still rotating. To validate the proposed unified control approach, simulations were performed for the two trajectories. For both cases, the UAV was able to follow the reference trajectory and executed them in the anticipated configurations, i.e. it flew in

a fixed-wing configuration in the first case and in an intermediate configuration in the second, with the front rotors not fully tilted forward and the tail rotor still providing lift. However, in the second case, the attitude, force and moment references, as well as the inputs, presented a quite irregular behaviour when compared to the first case where the UAV was in trim flight.

Finally, a tri-tiltrotor UAV, the *E-Flite Convergence VTOL*, was equipped with a PX4-compatible autopilot, the Pixhawk 4 Mini, and with the additional required components in order to be able to perform real flight tests. A power module was assembled to supply power to the motors, autopilot and other modules. The UAV was also fitted with a GPS module, a WiFi module and a radio receiver. Additionally, reflective markers to track the vehicle using a motion capture system were attached to the UAV. To verify the assembly was correct, a test flight was performed.

8.2 Future Work

There are some paths that can be explored in terms of future work.

To perform more accurate simulations and improve the controller performance, a good knowledge of the system model is necessary. As such, calculating the aerodynamic coefficients and other parameter values for the *E-Flite Convergence VTOL*, via fluid dynamics simulations or wind tunnel testing, for example, would be advantageous.

Another issue that requires further work is the computation of the orientation and angular velocity references. In the current approach, a nonlinear optimisation problem is formulated and solved at each time instant. As aforementioned, there is a problem related to the computation time, which may be excessive, and hence not viable for a real world application. It might also be the case that the solver does not find a solution. Therefore, this matter requires more research to find a better approach, possibly one with a closed-form solution.

Related to the control approach as well, is the problem of the control allocation. By also relying on a nonlinear optimisation to compute the input values, the issues are similar to those of the orientation reference generation (excessive computation time and the possibility of failure to find a solution). Moreover, the longitudinal and lateral dynamics were considered disproportionately, which was reasonable for the trajectories considered, but would not be for every trajectory. As such, devising a strategy that takes into account the force and moment references as a whole would be a line of research worth exploring.

In addition, expanding the unified control approach to be able to perform transitions from cruise flight to hover would be important, in order to complete the range of manoeuvres that are characteristic of hybrid UAV.

Finally, mounting a companion computer on the UAV to implement and test the control approach described in this dissertation, or an improved version, is a significant line of work to follow as well.

Bibliography

[1] B. J. Guerreiro, "REPLACE Project." [Online]. Available: http://replace.isr.tecnico.ulisboa.pt

[2] "Controller Diagrams · PX4 Developer Guide." [Online]. Available: https://dev.px4.io/master/en/flight_stack/controller_diagrams.html

[3] S. Ginter and R. Koenen, *Lockheed XFV-1 VTOL Fighter*, ser. Naval Fighters 32. Naval Fighters, 1996.

[4] S. Coleman, S. Ginter, B. J. Long, and B. Chana, *Convair XFY-1 Pogo*, ser. Naval Fighters No 27. Ginter Book, 1994.

[5] A. M. Thornborough, *Bell Boeing V-22 Osprey - Tiltrotor Tactical Transport*, ser. Aeroguide Special. Linewrights, 2004.

[6] "OGASSA OGS42V — UAVision Aeronautics." [Online]. Available: https://www.uavision.com/copy-of-ogassa-ogs42

[7] A. S. Saeed, A. B. Younes, C. Cai, and G. Cai, "A survey of hybrid Unmanned Aerial Vehicles," *Progress in Aerospace Sciences*, vol. 98, pp. 91–105, 4 2018.

[8] M. Hochstenbach, C. Notteboom, B. Theys, and J. De Schutter, "Design and control of an unmanned aerial vehicle for autonomous parcel delivery with transition from vertical take-off to forward flight - VertiKUL, a quadcopter tailsitter," *International Journal of Micro Air Vehicles*, vol. 7, no. 4, pp. 395–405, 12 2015.

[9] "Maribot Kungsfiskare - Amphibious Autonomous Drone - eVTOL — KTHAero." [Online]. Available: https://www.kthaero.com/mrlkf

[10] "Deutsche Post DHL Group — DHL Parcelcopter." [Online]. Available: https://www.dpdhl.com/en/media-relations/specials/dhl-parcelcopter.html

[11] Z. Liu, Y. He, L. Yang, and J. Han, "Control techniques of tilt rotor unmanned aerial vehicle systems: A review," *Chinese Journal of Aeronautics*, vol. 30, no. 1, pp. 135–148, 2 2017.

[12] D. A. Ta, I. Fantoni, and R. Lozano, “Modeling and control of a tilt tri-rotor airplane,” in *Proceedings of the American Control Conference*, 2012, pp. 131–136.

[13] G. R. Flores, J. Escareno, R. Lozano, and S. Salazar, “Quad-Tilting Rotor Convertible MAV: Modeling and Real-Time Hover Flight Control,” *J Intell Robot Syst*, vol. 65, pp. 457–471, 2012.

[14] G. Flores and R. Lozano, “Transition flight control of the quad-tilting rotor convertible MAV,” in *2013 International Conference on Unmanned Aircraft Systems, ICUAS 2013 - Conference Proceedings*, 2013, pp. 789–794.

[15] R. G. Hernandez-Garcia and H. Rodriguez-Cortes, “Transition flight control of a cyclic tiltrotor UAV based on the Gain-Scheduling strategy,” in *2015 International Conference on Unmanned Aircraft Systems, ICUAS 2015*. Institute of Electrical and Electronics Engineers Inc., 7 2015, pp. 951–956.

[16] D. A. Ta, I. Fantoni, and R. Lozano, “Modeling and control of a convertible mini-UAV,” in *IFAC Proceedings Volumes (IFAC-PapersOnline)*, vol. 44, no. 1 PART 1. IFAC Secretariat, 1 2011, pp. 1492–1497.

[17] L. Yu, D. Zhang, J. Zhang, and C. Pan, “Modeling and attitude control of a tilt tri-rotor UAV,” in *Chinese Control Conference, CCC*. IEEE Computer Society, 9 2017, pp. 1103–1108.

[18] B. Yuksek, A. Vuruskan, U. Ozdemir, M. A. Yukselen, and G. Inalhan, “Transition Flight Modeling of a Fixed-Wing VTOL UAV,” *Journal of Intelligent and Robotic Systems: Theory and Applications*, vol. 84, no. 1-4, pp. 83–105, 2016.

[19] P. Hartmann, C. Meyer, and D. Moormann, “Unified velocity control and flight state transition of unmanned tilt-wing aircraft,” *Journal of Guidance, Control, and Dynamics*, vol. 40, no. 6, pp. 1348–1359, 2017.

[20] J. Zhou, X. Lyu, Z. Li, S. Shen, and F. Zhang, “A unified control method for quadrotor tail-sitter UAVs in all flight modes: Hover, transition, and level flight,” in *IEEE International Conference on Intelligent Robots and Systems*, vol. 2017-Septe. Institute of Electrical and Electronics Engineers Inc., 12 2017, pp. 4835–4841.

[21] “Control Allocation: reworking the PX4 mixing system — PX4 Developer Summit Virtual 2020.” [Online]. Available: https://youtu.be/xjLM9whwjO4

[22] B. Siciliano and O. Khatib, *Handbook of Robotics*. Springer, 2016.

[23] A. J. Hanson, *Visualizing Quaternions: Series in Interactive 3D Technology*. Elsevier, 2006.

[24] H. K. Khalil, *Nonlinear Control*. Pearson Education Limited, 2015.

[25] ——, *Nonlinear Systems*. Upper Saddle River, New Jersey: Prentice Hall, 1996.

[26] R. Sepulchre, M. Janković, and P. V. Kokotović, *Constructive Nonlinear Control*. London: Springer London, 1997.

[27] G. Cai, B. M. Chen, and T. H. Lee, *Unmanned rotorcraft systems*. Springer, 2011.

[28] R. W. Beard and T. W. McLain, *Small unmanned aircraft: Theory and practice*. Princeton University Press, 2012.

[29] F. Kendoul, I. Fantoni, and R. Lozano, "Modeling and control of a small autonomous aircraft having two tilting rotors," in *Proceedings of the 44th IEEE Conference on Decision and Control, and the European Control Conference, CDC-ECC '05*, vol. 2005, 2005, pp. 8144–8149.

[30] Y. Long, L. Wang, and D. J. Cappelleri, "Modeling and global trajectory tracking control for an over-actuated MAV," *Advanced Robotics*, vol. 28, no. 3, pp. 145–155, 2 2014.

[31] "Pixhawk 4 Mini — PX4 User Guide." [Online]. Available: https://docs.px4.io/master/en/flight_controller/pixhawk4_mini.html

A

Model and Simulation Parameters

In this appendix, the values for the UAV model and simulation parameters are presented. The aerodynamic coefficients and other parameters related to the tiltrotor UAV, adapted from the fixed-wing UAV Aerosonde in [28], are shown in Table A.1. Modified or added parameters are marked with $(*)$. Parameters related to the controller are presented in Table A.2.

Table A.1: Simulation Tiltrotor UAV parameters

Parameter	Value
m	$13.5\,\text{kg}$
$\mathbf{J}$	$\begin{bmatrix} 0.8244 & 0 & 0.1204 \\ 0 & 1.135 & 0 \\ 0.1204 & 0 & 1.759 \end{bmatrix}\,\text{kg}\,\text{m}^2$
S	$0.55\,\text{m}^2$
b	$0.28956\,\text{m}$
c	$0.18994\,\text{m}$
S_{rotor}	$0.2027\,\text{m}^2$
ρ	$1.2682\,\text{kg/m}^3$
e_{Osw}	40.9
AR	15.24

Continued on next page

Table A.1 – continued from previous page

Parameter	Value
M	50
α_0	$0.4712\,\text{rad}$
C_{prop}	1.0
$C_{\text{Lift},0}$	0.28
$C_{\text{Lift},\alpha}$	3.45
$C_{\text{parasitic}}$	0.0437
C_{m_0}	-0.02338
C_{m_α}	-0.38
C_{m_e}	-0.5
C_{Y_a}	0
C_{Y_β}	-0.98
C_{l_a}	0.08
C_{l_β}	-0.12
C_{n_a}	0.06
C_{n_β}	0.25
$(*)$ k_{F}	1
k_{M}	0
$(*)$ $k_{\text{F,tr}}$	1.5
$k_{\text{M,tr}}$	0
$(*)$ $\mathbf{r}_1$	$\begin{bmatrix}0.1 & 0.72 & 0\end{bmatrix}^\mathsf{T}\,\text{m}$
$(*)$ $\mathbf{r}_2$	$\begin{bmatrix}0.1 & 0.-72 & 0\end{bmatrix}^\mathsf{T}\,\text{m}$
$(*)$ $\mathbf{r}_{\text{tr}}$	$\begin{bmatrix}-0.25 & 0 & 0\end{bmatrix}^\mathsf{T}\,\text{m}$
$(*)$ γ_{min}	$0\,\text{rad}$
$(*)$ γ_{max}	$5\pi/9\,\text{rad}$
$(*)$ $\gamma_{1,\text{min}}$	$0\,\text{rad}$
$(*)$ $\gamma_{1,\text{max}}$	$5\pi/9\,\text{rad}$
$(*)$ $\gamma_{2,\text{min}}$	$0\,\text{rad}$
$(*)$ $\gamma_{2,\text{max}}$	$5\pi/9\,\text{rad}$
$(*)$ $\delta_{\text{e,min}}$	$-\pi/3\,\text{rad}$
$(*)$ $\delta_{\text{e,max}}$	$\pi/3\,\text{rad}$
$(*)$ $\delta_{\text{a,min}}$	$-\pi/3\,\text{rad}$
$(*)$ $\delta_{\text{a,max}}$	$\pi/3\,\text{rad}$

Table A.2: Controller parameters

Parameter	Value
k_1	1
$k_{1,\text{I}}$	2
k_2	5
k_3	5
k_4	10
k_ω	0.1
θ_{min}	$-0.1745\,\text{rad}$
θ_{max}	$0.1745\,\text{rad}$
$\omega_{1,\text{max}}$	$100\,\text{rad/s}$
$\omega_{2,\text{max}}$	$100\,\text{rad/s}$
$\omega_{\text{tr,max}}$	$100\,\text{rad/s}$